

Volume 72, issue 2, September 2014

45 articles in this issue

Aims and scope

Multimedia Tools and Applications publishes original research articles on multimedia development and system support tools, and case studies of multimedia applications. Experimental and survey articles are appropriate for the journal. The journal is intended for academics, practitioners, scientists and engineers who are involved in multimedia system research, design and applications. All papers are peer reviewed.

Editors

Editor-in-Chief:

Borko Furht, *Dept. of Computer Science and Engineering, Florida Atlantic University, USA*

Section Editors:

Harry Agius, *Brunel University London, United Kingdom*

Jungong Han, *Aberystwyth University, United Kingdom*

Fabio Narducci, *University of Salerno, Italy*

Maria Da Graça Pimentel, *University of São Paulo, Brazil*

Weisong Shi, *University of Delaware, Wilmington, Delaware, USA*

Associate Editors:

Sambit Bakshi, *National Institute of Technology Rourkela, India*

Carmen Bisogni, *University of Salerno, Italy*

Wei Cheng, *University of Washington, Tacoma, Washington, USA*

Zheng Dong, *Wayne State University, Detroit, Michigan, USA*

Song Fu, *University of North Texas, Denton, Texas, USA*

Chiara Galdi, *EURECOM, Sophia Antipolis, France*

Dalong Li, *Torc Robotics, USA*

Dongfang Liu, *Rochester Institute of Technology, Rochester, New York, USA*

Jianping Wang, *City University of Hong Kong, China*

Dewei Yi, *University of Aberdeen, UK*

Qiang Zhang, *Xidian University, China*

Editorial Board:

Marios C. Angelides, *Brunel University London, United Kingdom*

Marco Anisetti, *University of Milano, Italy*

Andrew Bagdanov, *University of Florence, Italy*

Lamberto Ballan, *Stanford University, USA*

Jenny Benois-Pineau, *University of Bordeaux, France*

Marco Bertini, *University of Florence, Italy*

Bharat Bhargava, *Purdue University, USA*

Alberto del Bimbo, *Università di Firenze, Italy*

Susanne Boll, *University of Oldenburg, Germany*

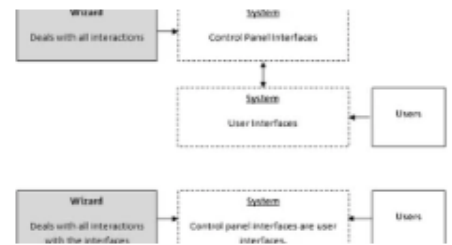
Ying Cai, *Iowa State University, Ames, Iowa, USA*
Aniello Castiglione, *University of Naples, Italy*
Pablo Cesar, *Centrum Wiskunde & Informatica, Netherlands*
Amit Chakraborty, *Siemens Corporate Research, USA*
Shu-Ching Chen, *Florida International University, Miami, Florida, USA*
Tat-Seng Chua, *National University of Singapore*
Ernesto Damiani, *University of Milano, Italy*
Antitza Dantcheva, *INRIA, France*
Chabane Djeraba, *LIFL Laboratory, France*
Schahram Dustdar, *Vienna University of Technology, Wien, Austria*
Abdulmotaleb El Saddik, *University of Ottawa, Canada*
Ben Falchuk, *Vencore Labs, USA*
Marco Furini, *University of Modena and Reggio Emilia, Italy*
Ombretta Gaggi, *University of Padua, Italy*
David C. Gibbon, *AT&T Labs - Research, USA*
Yihong Gong, *NEC, USA*
Sonja Grgic, *University of Zagreb, Croatia*
M. Shamim Hossain, *King Saud University, Saudi Arabia*
Kien A. Hua, *University of Central Florida, USA*
Benoit Huet, *Institut Eurecom, France*
Horace H.S. Ip, *City University of Hong Kong*
Ebroul Izquierdo, *Queen Mary, University of London, United Kingdom*
Ramesh Jain, *University of California, Irvine, USA*
Rongrong Ji, *Xiamen University, China*
Shuqiang Jiang, *Chinese Academy of Sciences, China*
Hari Kalva, *Florida Atlantic University, Boca Raton, Florida, USA*
Shunsuke Kamijo, *University of Tokyo, Japan*
Ahmed Karmouch, *University Ottawa, Canada*
Harald Kosch, *University of Passau, Germany*
Clement Leung, *Hong Kong Baptist University, Hong Kong*
T.D.C. Little, *Boston University, USA*
Huadong Ma, *Beijing University of Posts & Telecommunications, PR of China*
Hong Man, *Stevens Institute of Technology, Hoboken, New Jersey, USA*
Oge Marques, *Florida Atlantic University, Boca Raton, Florida, USA*
Liam M. Mayron, *Florida Institute of Technology, Florida, USA*
Michele Nappi, *University of Salerno, Italy*
Vincent Oria, *New Jersey Institute of Technology, New Jersey, USA*

Charles B. Owen, *Michigan State University, USA*
Dragutin Petkovic, *San Francisco State University, USA*
Giuseppe Polese, *University of Salerno, Italy*
Jorge Posada, *Vicomtech Research Centre, Spain*
B. Prabhakaran, *University of Texas at Dallas, USA*
Martin Reisslein, *Arizona State University, Tempe, Arizona*
Marco Rocchetti, *University of Bologna, Italy*
Simone Santini, *University of California at San Diego, USA*
Shin'ichi Satoh, *National Institute of Informatics, Tokyo, Japan*
Klaus Schöffmann, *Klagenfurt University, Austria*
Lorenzo Seidenari, *University of Florence, Italy*
Ali Asghar Nazari Shirehjini, *Karlsruhe Institute of Technology, Germany*
Scott M. Stevens, *SEI, Carnegie Mellon University, USA*
Jinhui Tang, *Nanjing University of Science and Technology, P.R. China*
Yoshiyasu Takefuji, *Keio University, Japan*
Christian Timmerer, *Klagenfurt University, Austria*
Tiberio Uricchio, *University of Florence, Italy*
Jingdong Wang, *Microsoft Research Asia, China*
Meng Wang, *Hefei University of Technology, China*
Qi Wang, *Northwestern Polytechnical University, China*
Lars Wolf, *Technical University Braunschweig, Germany*
Changsheng Xu, *NLPR, Chinese Academy of Sciences, China*
Hanwang Zhang, *National University of Singapore, Singapore*
Zhiyong Zhang, *Henan University of Science and Technology, China*
Roger Zimmermann, *National University of Singapore, Singapore*
Ce Zhu, *Nanyang Technological University, Singapore*

[Using wizard-of-oz method to build multipurpose platform for domestic ambient media research and applications](#)

Andol X. Li & John V. H. Bonner

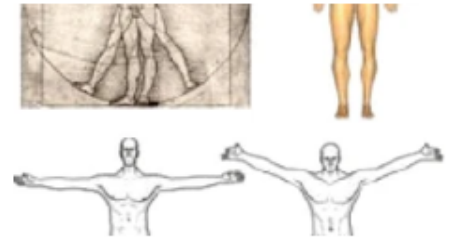
OriginalPaper | Published: 13 March 2013 | Pages: 1011 - 1026



[Symmetry discovery and retrieval of nonrigid 3D shapes using geodesic skeleton paths](#)

Chunyuan Li & A. Ben Hamza

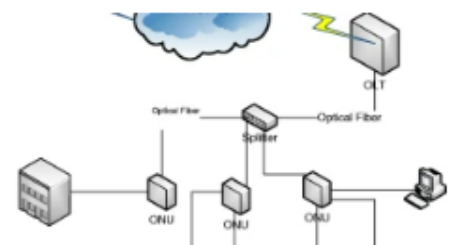
OriginalPaper | Published: 15 March 2013 | Pages: 1027 - 1047



[IFCS: an intelligent fast channel switching in IPTV over PON based on human behavior prediction](#)

Ali Athari Beyragh & Akbar Ghaffarpour Rahbar

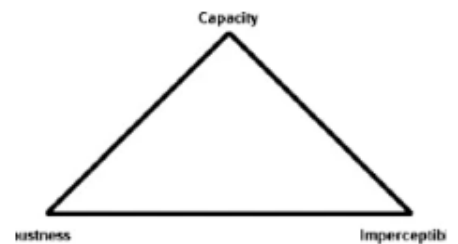
OriginalPaper | Published: 20 March 2013 | Pages: 1049 - 1071



[Chaos based Zero-steganography algorithm](#)

Muhammad Bilal, Sana Imtiaz ... Shahzad Asif

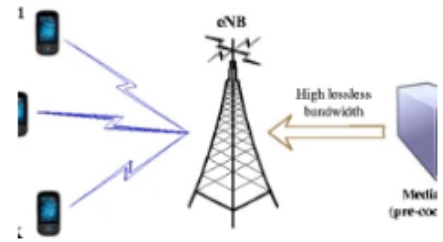
OriginalPaper | Published: 20 March 2013 | Pages: 1073 - 1092



QoE-based cross-layer design for video applications over LTE

Ying Ju, Zhaoming Lu ... Wenmin Ma

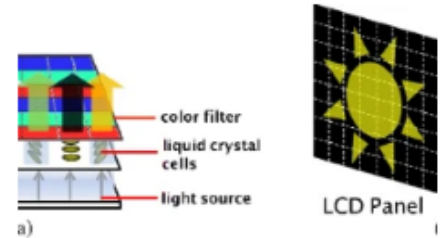
OriginalPaper | Published: 24 March 2013 | Pages: 1093 - 1113



High power-saving and fidelity-conserving object-based local dimming for LCD systems with LED-based backlight units

Aldhino Anggorosesar & Young-Jin Kim

OriginalPaper | Published: 24 March 2013 | Pages: 1115 - 1141

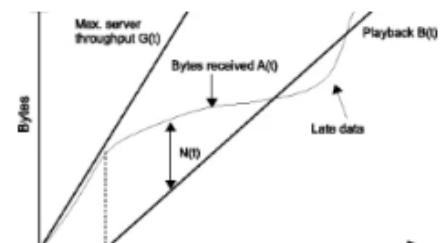


Performance of HTTP video streaming under different network conditions

Arkadiusz Biernacki & Kurt Tutschku

OriginalPaper | [Open Access](#) | Published: 26 March 2013 |

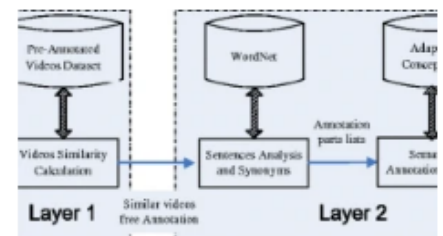
Pages: 1143 - 1166



A framework for automatic semantic video annotation

Amjad Altadmri & Amr Ahmed

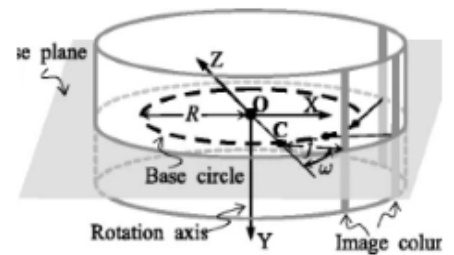
OriginalPaper | Published: 28 March 2013 | Pages: 1167 - 1191



[Sensitivity analysis of pose recovery from multi-center panoramas](#)

Fay Huang

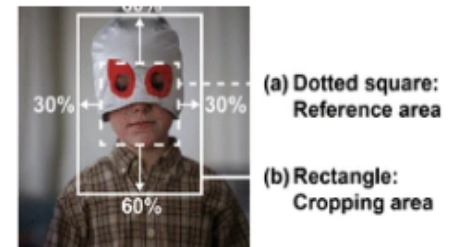
OriginalPaper | Published: 29 March 2013 | Pages: 1193 - 1213



[FaceCAPTCHA: a CAPTCHA that identifies the gender of face images unrecognized by existing gender classifiers](#)

Jonghak Kim, Sangtae Kim ... KwangYun Wahn

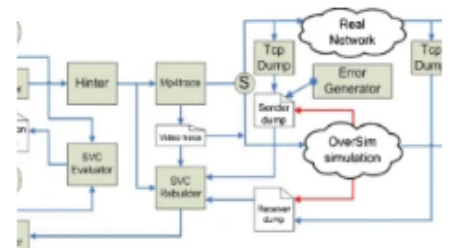
OriginalPaper | Published: 02 April 2013 | Pages: 1215 - 1237



[End-to-end transmission of scalable video contents: performance evaluation over EvalSVC—a new open-source evaluation platform](#)

Tien Anh Le & Hang Nguyen

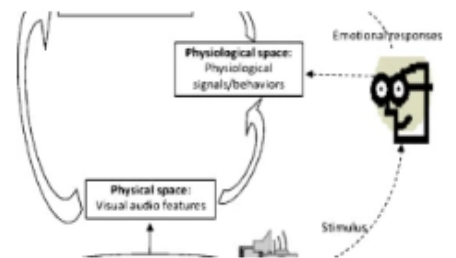
OriginalPaper | Published: 06 April 2013 | Pages: 1239 - 1256



[Hybrid video emotional tagging using users' EEG and video content](#)

Shangfei Wang, Yachen Zhu ... Qiang Ji

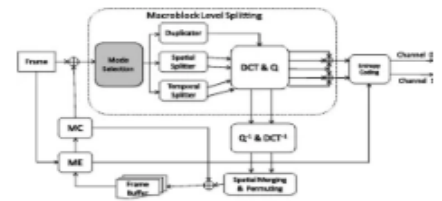
OriginalPaper | Published: 10 April 2013 | Pages: 1257 - 1283



[Rate-distortion optimized mode selection method for multiple description video coding](#)

Yu-Chen Sun & Wen-Jiin Tsai

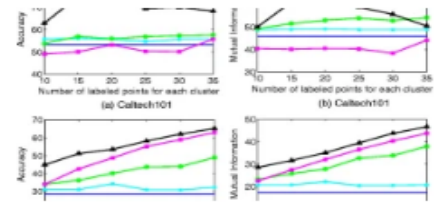
OriginalPaper | Published: 19 April 2013 | Pages: 1411 - 1439



[Semi-supervised non-negative matrix factorization for image clustering with graph Laplacian](#)

Yangcheng He, Hongtao Lu & Saining Xie

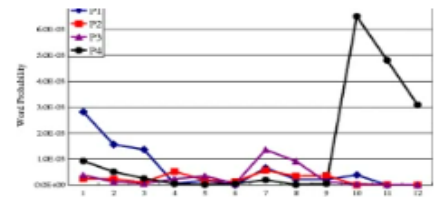
OriginalPaper | Published: 19 April 2013 | Pages: 1441 - 1463



[Leveraging topical and positional cues for language modeling in speech recognition](#)

Hsuan-Sheng Chiu, Kuan-Yu Chen & Berlin Chen

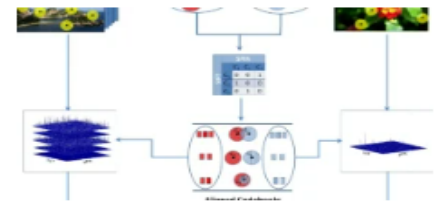
OriginalPaper | Published: 19 April 2013 | Pages: 1465 - 1481



[Aligning codebooks for near duplicate image detection](#)

Sebastiano Battiato, Giovanni Maria Farinella ... Daniele Ravi

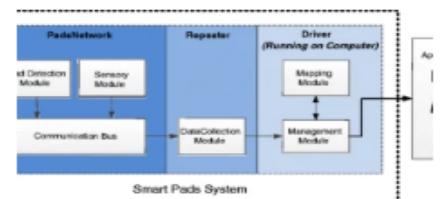
OriginalPaper | Published: 21 April 2013 | Pages: 1483 - 1506



[SmartPads: a plug-N-play configurable tangible user interface](#)

Basim Hafidh, Hussein Al Osman ... Abdulmotaleb El Saddik

OriginalPaper | Published: 21 April 2013 | Pages: 1507 - 1530



[Hybrid shape descriptor and meta similarity generation for non-rigid and partial 3D model retrieval](#)

Bo Li, Afzal Godil & Henry Johan

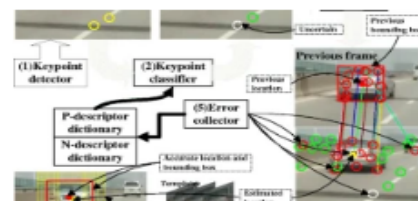
OriginalPaper | Published: 23 April 2013 | Pages: 1531 - 1560



[On-road vehicle tracking using keypoint-based representation and online co-training](#)

Shuo Yang, Jie Xu ... Minghui Wang

OriginalPaper | Published: 25 April 2013 | Pages: 1561 - 1583



[Ambient mesoscale weather forecasting system featuring mobile augmented reality](#)

Jenq-Shiou Leu, Kuan-Wu Su & Cheng-Tsung Chen

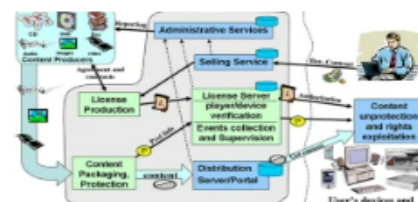
OriginalPaper | Published: 25 April 2013 | Pages: 1585 - 1609



[Exploiting P2P scalability for grant authorization in digital rights management solutions](#)

Pierfrancesco Bellini, Paolo Nesi & Fabio Pazzaglia

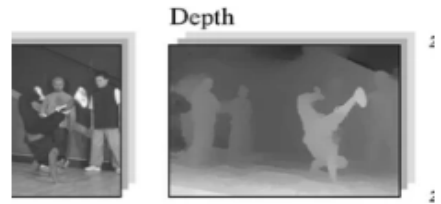
OriginalPaper | [Open Access](#) | Published: 26 April 2013 | Pages: 1611 - 1637



[Efficient depth coding in 3D video to minimize coding bitrate and complexity](#)

Liquan Shen & Zhaoyang Zhang

OriginalPaper | Published: 26 April 2013 | Pages: 1639 - 1652



[TuBeck: a novel peer-to-peer streaming system with Loopback-MDC for scalable H.264/AVC videos](#)

Chow-Sing Lin, Rong-Hua Chang & Jhe-Wei Lin

OriginalPaper | Published: 27 April 2013 | Pages: 1653 - 1679

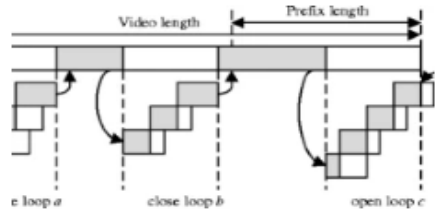
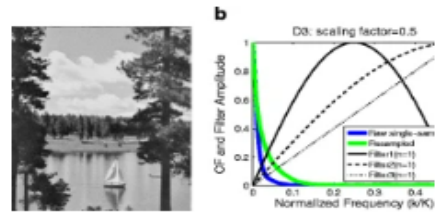


[Image resampling detection based on texture classification](#)

Xiaodan Hou, Tao Zhang ... Xin Ping

OriginalPaper | Published: 28 April 2013 | Pages: 1681 - 1708



[Multiple color space channel fusion for skin detection](#)

Rehanullah Khan, Allan Hanbury ... Amjad Ali

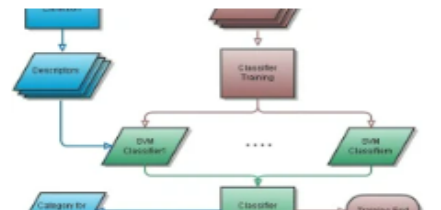
OriginalPaper | Published: 28 April 2013 | Pages: 1709 - 1730



[Evidence-based SVM fusion for 3D model retrieval](#)

Zongmin Li, Zijian Wu ... Jianping Fan

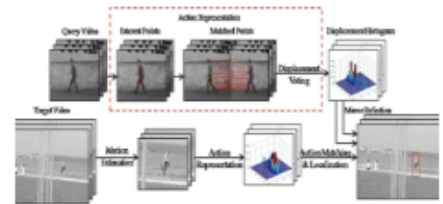
OriginalPaper | Published: 01 May 2013 | Pages: 1731 - 1749



[One example based action detection in hough space](#)

Lishen Pei, Mao Ye ... Guanjun Guo

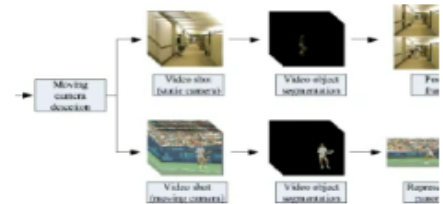
OriginalPaper | Published: 01 May 2013 | Pages: 1751 - 1772



[Object segmentation and key-pose based summarization for motion video](#)

Zhiqiang Tian, Jianru Xue ... Nanning Zheng

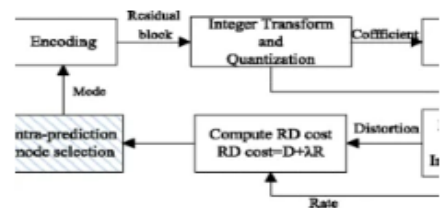
OriginalPaper | Published: 01 May 2013 | Pages: 1773 - 1802



[An efficient mode decision algorithm for H.264/AVC intra prediction](#)

Yonghong Kuo, Jiefeng Yang & Jian Chen

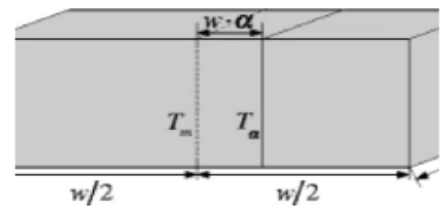
OriginalPaper | Published: 03 May 2013 | Pages: 1803 - 1821



[Fast BVH construction and refit for ray tracing of dynamic scenes](#)

Mingqiang Yin & Shiqi Li

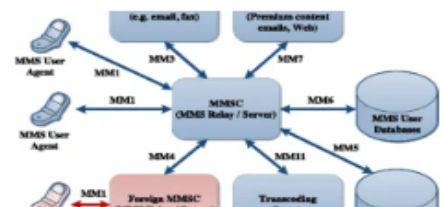
OriginalPaper | Published: 03 May 2013 | Pages: 1823 - 1839



[Quality-aware predictor-based adaptation of still images for the multimedia messaging service](#)

Steven Pigeon & Stéphane Coulombe

OriginalPaper | Published: 07 May 2013 | Pages: 1841 - 1865



[Multi-secret visual cryptography with deterministic contrast](#)

Bin Yu & Gang Shen

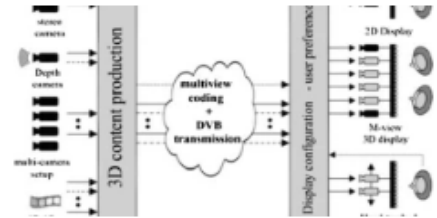
OriginalPaper | Published: 08 May 2013 | Pages: 1867 - 1886



[A taxonomy of depth map creation methods used in multiview video compression](#)

Seyed Morteza Ayatollahi, Amir Masoud Eftekhari Moghadam & Monireh Sadat Hosseini

OriginalPaper | Published: 08 May 2013 | Pages: 1887 - 1909



[Embedding neural networks for semantic association in content based image retrieval](#)

Aun Irtaza, M. Arfan Jaffar ... Tae-Sun Choi

OriginalPaper | Published: 09 May 2013 | Pages: 1911 - 1931



[SVM correction based geometrically invariant digital watermarking algorithm](#)

Xiang-yang Wang, Chun-peng Wang ... Hong-ying Yang

OriginalPaper | Published: 10 May 2013 | Pages: 1933 - 1960

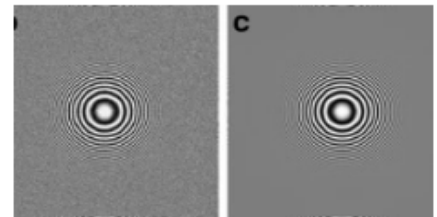
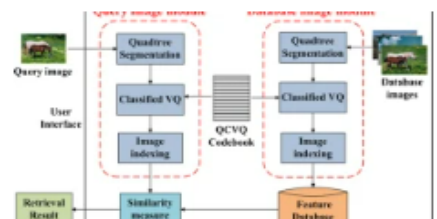


[Image retrieval based on quadtree classified vector quantization](#)

Hsin-Hui Chen, Jian-Jiun Ding & Hsin-Teng Sheu

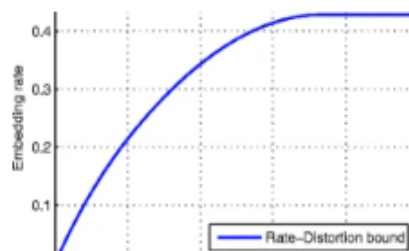
OriginalPaper | Published: 12 May 2013 | Pages: 1961 - 1984



[Recursive code construction for reversible data hiding in DCT domain](#)

Biao Chen, Weiming Zhang ... Nenghai Yu

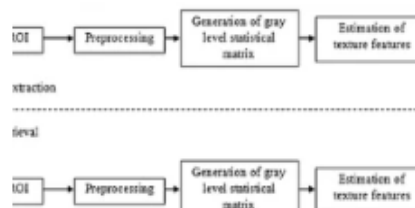
OriginalPaper | Published: 17 May 2013 | Pages: 1985 - 2009



[Texture feature extraction using gray level statistical matrix for content-based mammogram retrieval](#)

D. Abraham Chandy, J. Stanly Johnson & S. Easter Selvan

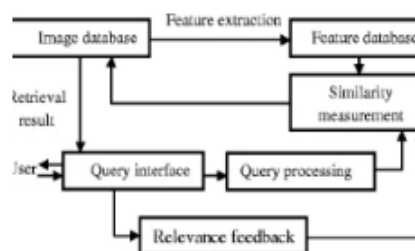
OriginalPaper | Published: 25 May 2013 | Pages: 2011 - 2024



[A short-term learning approach based on similarity refinement in content-based image retrieval](#)

Asma Shamsi, Hossein Nezamabadi-pour & Saeid Saryazdi

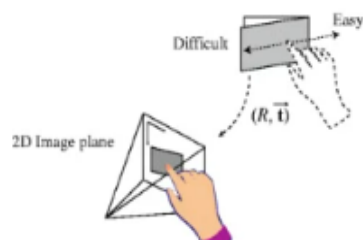
OriginalPaper | Published: 26 May 2013 | Pages: 2025 - 2039



[Haptic interaction with objects in a picture based on pose estimation](#)

Seung-Chan Kim & Dong-Soo Kwon

OriginalPaper | Published: 26 May 2013 | Pages: 2041 - 2062



A visible wavelet watermarking technique based on exploiting the contrast sensitivity function and noise reduction of human vision system

Min-Jen Tsai · Jung Liu · Jin-Sheng Yin · Imam Yuadi

Published online: 13 April 2013

© Springer Science+Business Media New York 2013

Abstract With the widespread use of the Internet and the rapid development of digital technologies, copyright protection of multimedia content has become an important issue. Among the available technologies, digital watermarking techniques are regarded as a solution to the property right protection for multimedia resources. To evaluate the performance of a visible watermarking technique, robustness and perceptual translucence are two essential criteria for the watermark applications. In order to get the best trade-off between the embedding energy of a watermark and perceptual translucence, this study presents a technique named ICOCOA (innovated content and contrast aware) by exploiting the contrast sensitivity function (CSF) and noise reduction of human vision system in the wavelet domain. Another novel idea of this work is to propose the innovated CSF masking (I-CSF) curve which provides better weight perception where a game-theoretic architecture can be leveraged to determine the best I-CSF masking for the watermarked image. The experimental results demonstrate that the proposed approach not only provides a good translucent quality of the watermark but also achieves the robustness against the common image processing operations.

Keywords Copyright protection · Contrast Sensitivity Function (CSF) · Digital watermarking · Human Visual System (HVS) · Noise Visibility Function (NVF) · Wavelet

1 Introduction

In recent years, due to the advancement of digital technologies and rapid communication network deployment, digital images can be widely distributed and duplicated on the Internet or via other digital devices. There is an urgent demand for techniques to protect the digital data sources and to prevent unauthorized duplication or tampering. Various techniques including watermarking have been introduced in effort to deal with these increasing

M.-J. Tsai (✉) · J. Liu · J.-S. Yin · I. Yuadi
Institute of Information Management, National Chiao Tung University, 1001 Ta-Hsueh Road,
Hsin-Chu 300 Taiwan, Republic of China
e-mail: mjtsai@cc.nctu.edu.tw

concerns. Therefore, digital watermarking technology has emerged as an effective solution to protect the digital content from unauthorized copying, since it makes possible by embedding the secret information in the digital content for the identification of the copyright owner [7].

Different watermarking methods have been proposed to protect copyright ownership and they can be classified into two categories: spatial domain and transform domain techniques. In spatial domain methods of [12, 36], the watermark is achieved by directly modifying the pixel values of the host image. In transform domain schemes of [17, 22, 33], the host image is first converted into frequency domain by using transformation methods such as the Discrete Cosine Transform (DCT), Discrete Fourier Transform (DFT) or Discrete Wavelet Transform (DWT), etc. The watermark is then scaled and embedded in the transformed coefficients to obtain the watermarked image after inverse transform. Among these methods, spatial domain methods are simple and fast, but are not robust against attacks. In comparison, transform domain based watermarking techniques are more robust and suitable for many applications [22, 27].

On the other hand, the visible watermarking is an active way to protect copyrights; it not only discourages pirating and prevents attempts of copyright violations but also recognizes the ownership of multimedia resources directly. This type of digital watermarks is immediately viewable without any mathematical calculation but it has encountered the problems of easy detection of watermark location and watermark removal attack.

Many researchers have proposed various visible watermarking schemes to protect copyrights. From the literature survey, Chen [5] used a statistic approach to develop a visible watermarking mechanism in the pixel domain. Chen et al. [6] described an approach for adaptive visible watermarking based on the analysis of the threshold value of the image using Otsu's threshold to select the best embedding strength of the watermark at a particular position. An et al. [2] developed a pragmatic framework for RRW (robust reversible watermarking) via clustering and EPWM (enhanced pixel-wise masking). Huang et al. [13] proposed a UVW (unseen visible watermarking) schemes which auxiliary information can be delivered without any overhead deployment. Their approach is to deliver auxiliary information visually, not for printed document. However, visible watermarking technique should be applied for printed publications which will be the focus in this study. On the other hand, histogram-based lossless data embedding [10] is secure for copyright protection if side information transmission is available. Feature-based image watermarking scheme [11] which aims to survive various geometric distortion also have attracted attention for researchers.

Tsai and Liu [27] proposed a wavelet-based image watermarking to improve the performance of image watermarking by human visual system (HVS) model and neural networks. First, they derived the allowable visibility ranges of the HVS in a wavelet-transformed image and they exploited the ranges to compute the adaptive embedding strengths of the watermark. Artificial neural network (ANN) technique is later applied to memorize the relationships between the original wavelet coefficients and its watermark version. Consequently, the trained ANN is utilized for estimating the watermark without the original image. Huang and Tang [14] presented a contrast sensitive visible watermarking scheme with the assistance of HVS. They calculated the contrast sensitive function (CSF) mask from discrete wavelet transform domain and used a square function to determine the mask weights for each sub-band. At last, they adjusted the embedding weights based on the block classification of the texture sensitivity of HVS. Tsai [25] leveraged Huang and Tang's study [14] to utilize the contrast-sensitive function, noise visible function of perceptual model, and fine tune the basis function amplitudes of DWT coefficients for the best quality of perceptual translucence

and noise reduction. After thorough surveys, above mentioned techniques still need to set thresholds to avoid too much watermark energy in the low frequency bands [14, 25]. In brief, the previous works have partially resolved the following issues but not all of them:

- **Translucence:** The embedded watermark pattern should not visually interfere with the host image which can still remain high image fidelity.
- **Clarity and unobtrusiveness:** Since the applications of visible watermarking are often limited to content browsing or previewing, content viewers are annoyed at degraded visual quality. Therefore, the embedded patterns should be unobtrusive and identifiable perceptually which are resistant to possible attacks. However, the robustness of watermarking and quality of the digital content are generally conflicted with each other.

Therefore, how to resolve the above issues and determine the best trade-off between the intensity of embedded watermark and the perceptual translucence for visible watermark is becoming a subject of importance [14, 18, 25–28]. The goal of this paper is to present an innovated visible watermarking algorithm named ICOCOA (Innovated COntent and COntast Aware) with a novel contrast sensitivity function masking for wavelet based watermarking method which considers the characteristics in different frequency domain. The organization of this paper is as follows. Section 2 introduces the related method of CSF and NVF. In section 3, we will give the detailed description of the proposed ICOCOA watermarking technique. Sections 4 and 5 will present simulation results with discussion and conclusions respectively.

2 Background

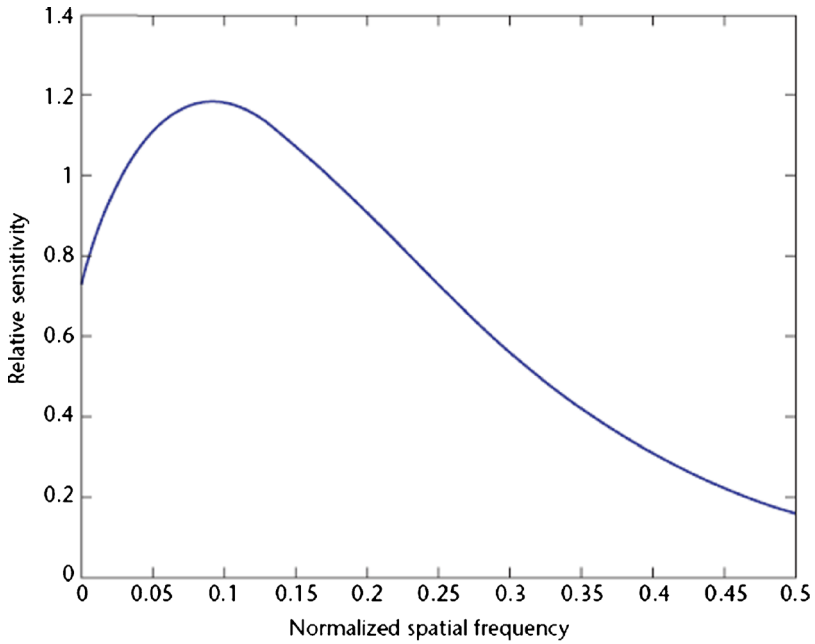
For the visible watermarking applications, robustness and translucence are the most important elements in the watermarking techniques, but unfortunately they are in confliction with each other. Human Visual System (HVS) is the key factor in providing the good translucence of the watermarked image and better robustness [14, 25, 26]. HVS research offers the mathematical models about how humans see the world and psychovisual studies have shown that human vision has different sensitivity from various spatial frequencies (frequency sub-bands). In this study, the HVS by using the CSF and NVF is integrated and will be explained in brief as following:

2.1 CSF (Contrast Sensitive Function)

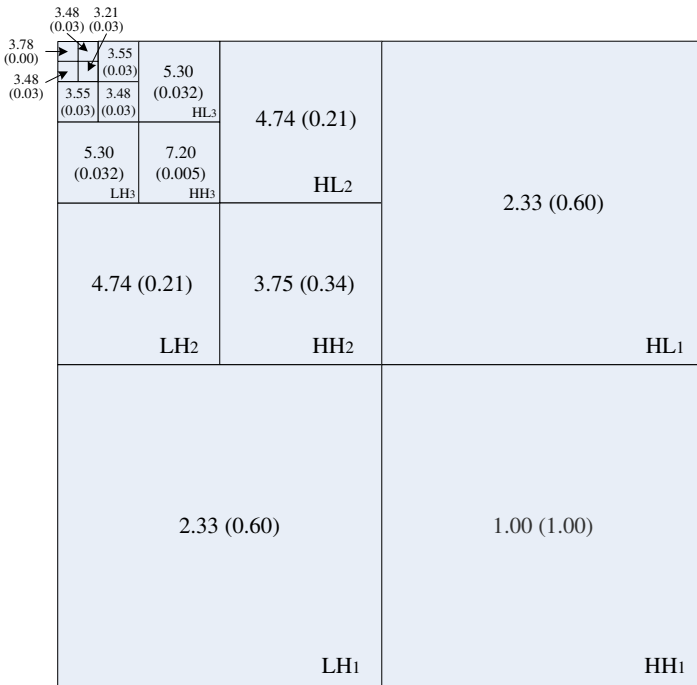
Mannos and Sakrison [18] originally presented a model of the CSF for luminance (or grayscale) images is given as follows:

$$H(f) = 2.6 \times (0.192 + 0.114 \times f) \times e^{-(0.114 \times f)^{1.1}} \quad (1)$$

where $f = \sqrt{f_x^2 + f_y^2}$ is the spatial frequency in cycles/degree of visual angle (f_x and f_y are the spatial frequencies in the horizontal and vertical directions, respectively). Figure 1(a) depicts the CSF curve which characterizes luminance sensitivity of the HVS as a function of spatial frequency. According to the CSF curve, we can see that the HVS is most sensitive to normalized spatial frequencies between 0.025 and 0.125 and less sensitive to low and high frequencies.



(a)



(b)

Fig. 1 **a** Luminance of contrast sensitive function. **b** DWT CSF mask with 11 unique weights after five-level wavelet pyramidal decomposition. $r_{\lambda,\theta}(\beta_{\lambda,\theta})$ values for each level λ are indicated at the center of each band

CSF masking [3, 16] is one way to apply the CSF in the discrete wavelet domain. CSF masking refers to the method of weighting the wavelet coefficients relative to their perceptual importance. In [3], the DWT CSF mask utilizes the information in all of the approximation sub-bands as well as all of the detail sub-bands to yield 11 unique weights in the mask. All of the weights are normalized so that the lowest weight is equal to one. The 11 weights of DWT CSF mask are shown in Fig. 1(b) after 5-level wavelet pyramidal DWT decomposition and the HVS is most sensitive to the distortion in mid-frequency regions (level 3) and sensitivity falls off as the frequency value drifts on both sides (level 1, 2, 4 and 5). The square function in [14] is applied to approximate the effect of CSF masking. The adequate modulation rate $\beta_{\lambda,\theta}$ for each sub-band is determined by:

$$\beta_{\lambda,\theta} = 0.01 + \frac{(7.20 - r_{\lambda,\theta})^2}{7.20^2} \quad (2)$$

where $r_{\lambda,\theta}$ represents the wavelet coefficient CSF of the perceptual importance weight for each sub-band where $\lambda(=1, 2, 3, 4, 5)$ denotes the decomposition level and $\theta(=1, 2, 3, 4, 5)$ is the orientation.

2.2 NVF (Noise Visibility Function)

Alexander et al. [1] presented a stochastic approach based on the computation of a NVF that characterizes the local image properties and identifies texture and edge regions. This allows us to determine the optimal watermark locations and strength for the watermark embedding stage. The adaptive scheme based on NVF calculated from stationary GG model is superior to other schemes, which is defined as follows:

$$NVF_{x,y} = \frac{w_{x,y}}{w_{x,y} + \sigma_I^2} \quad (3)$$

where $w_{x,y} = \gamma[\eta(\gamma)]^\gamma / \|r_{x,y}\|^{2-\gamma}$ and σ_I^2 is the global variance of the original image. $\eta(\gamma) = \sqrt{\Gamma(3/\gamma)/\Gamma(1/\gamma)}$, $\Gamma(s) = \int_0^\infty e^{-u} u^{s-1} du$ (gamma function) and $r_{x,y} = \frac{I_{x,y} - \bar{I}_{x,y}}{\sigma_I}$, γ is the shape parameter and $r_{x,y}$ is determined by the local mean and the local variance. For most of real images, the shape parameter is in the range $0.3 \leq \gamma \leq 1$. In our scheme, the estimated shape parameter for $\gamma=0.65$, and width of window is 1.

Next section, we will further clarify the goal of the study and describe the proposed ICOCOA watermark algorithm.

3 The proposed ICOCOA watermarking scheme

In order to improve the performance of watermarks in practice and provide an adaptive watermarking technique without threshold settings in different discrete wavelet domain, we not only develop a suitable perceptual weighting of wavelet coefficients based on traditional CSF which can resolve the problem of complex threshold settings but also propose a novel watermarking scheme named ICOCOA which leverages the knowledge of CSF and NVF for providing the good perceptual significance of visible watermark. The details will be explained in the following.

3.1 I-CSF (Innovated CSF)

The property of CSF is the fundamental spatiochromatic measure of the HVS while HVS is more sensitive in mid-frequency regions. Therefore, the principle of watermark embedding is to embed low intensity of visible watermark in high sensitivity regions and vice versa. In addition, the perceptual quality of the watermarked image will be affected directly by the low frequency signals during the embedding process. Consequently, less watermarked energy should be embedded in the wavelet coefficients of the LH, HL and HH sub-bands of the low and middle wavelet decomposition level (level 5, level 4 and level 3). According to such observation, we can draw the inverse CSF curve as shown in Fig. 2 which can help us to design a suitable watermark weighting curve.

Moreover, we found that the square function curve applied in [14, 25] dose not match the perfect inverse CSF curve as shown in Fig. 2 so they suddenly have a problem that they need to set certain thresholds to avoid adding too much energy in the low DWT frequency domains. In order to solve this issue and obtain the better watermarked image for HVS that contains the characteristics of robustness and translucence, we use the interpolation method to construct the innovated CSF masking to improve the HVS model for better image quality. From above discussion, we have proposed an innovated CSF masking (I-CSF), which is defined in formula (4).

$$I\text{-CSF} = (I - H(f)) \times f^\delta \tag{4}$$

where f is the approximation frequency value that is estimated from [14]. $H(f)$ is calculated by Eq. (1) and δ is the watermark weighting factor. In Fig. 2, we observe that the proposed curve of $\delta=0.5$ has high sensitivity weighting in the low DWT frequency that will cause the acute problem of image quality degradation. On the other hand, the embedded patterns will

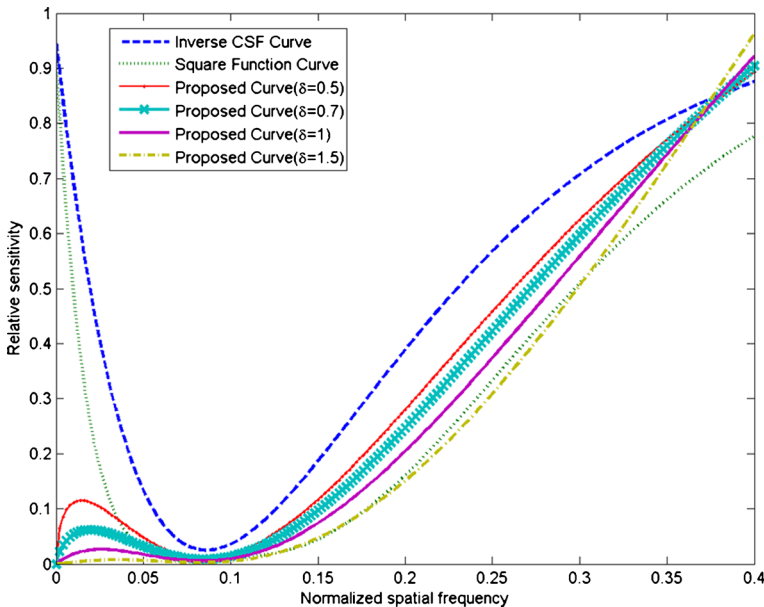


Fig. 2 Different weight perceptual curves of inverse CSF, square function and proposed curves

not be perceptually identifiable for $\delta=1.5$. Therefore, the best watermark weighting parameter for δ is decided at 0.7 which will be explained in details in section 4.1.

Figure 3 illustrates the corresponding coefficients of the I-CSF masking values of $\delta=0.7$ in different DWT level and orientation.

3.2 The ICOCOA watermarking embedding algorithm

We thus present a technique, ICOCOA, to tackle the challenges so that performance of visible watermarking can be improved. ICOCOA algorithm leverages the study of [25] and Fig. 4 illustrates the flow chart of ICOCOA watermarking scheme. The watermark embedding procedures are briefly described as following steps.

- Step 1 The watermark is embedded in the wavelet coefficients of the luminance Y , thus the first step of our algorithm is the conversion of the RGB color space into the YCrCb color space. A lot of watermarking schemes embed data in the luminance/intensity due to the fact that the Human Visual System (HVS) uses most of its bandwidth on perceptual brightness. This is the general approach for color watermarking. Since [14, 25] also adopted this approach, this research follows the rule to make the fair comparison.
- Step 2 By using Bi9/7 filter from [34], compute the 2-D wavelet coefficients of the luminance Y component from original color image and grayscale logo watermark image. In this paper we have chosen a wavelet decomposition on $L=5$ resolution levels.
- Step 3 The watermark is embedded in the wavelet coefficients of the LH, HL and HH sub-bands of the different wavelet decomposition level. Therefore, we

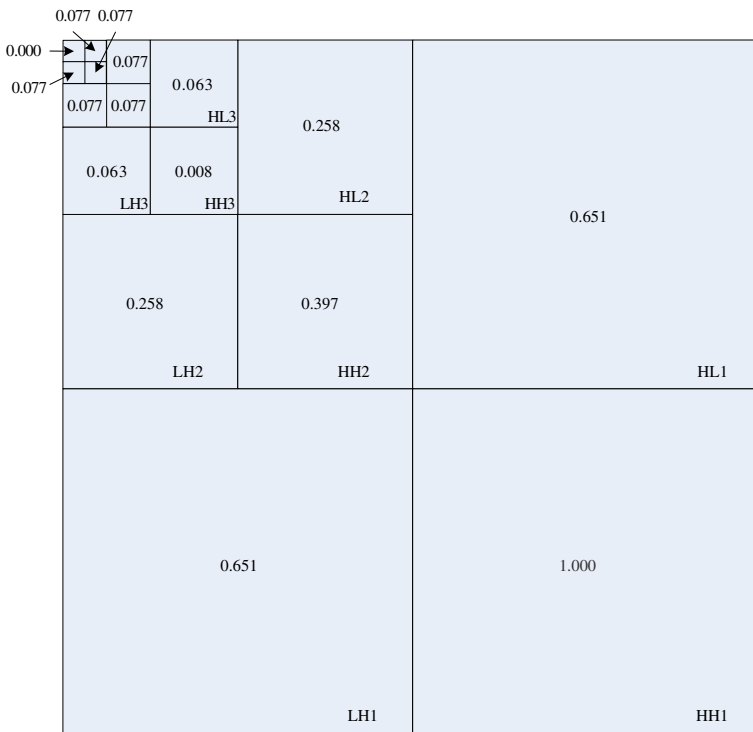


Fig. 3 The I-CSF masking with 11 unique weights after five-level wavelet pyramidal decomposition

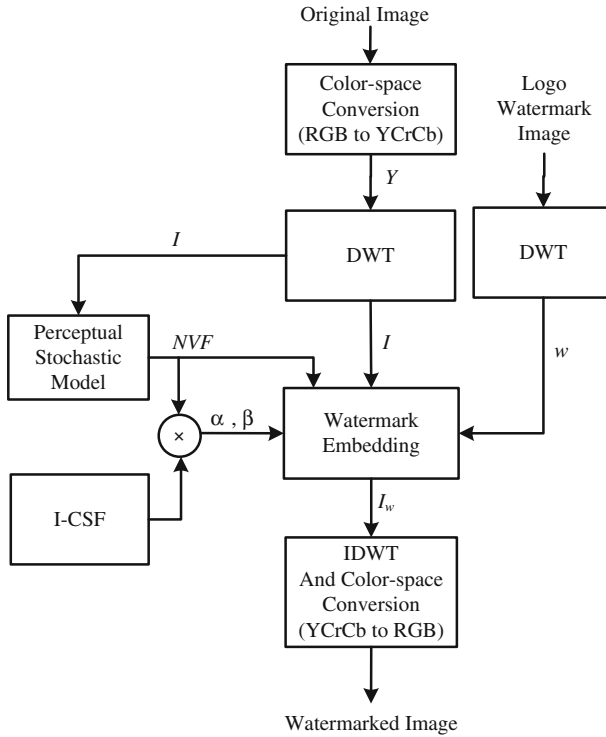


Fig. 4 The flow chart of ICOCOA visible watermarking algorithm

will modify the DWT coefficients of the host image by using the following equation:

$$I_{x,y}^w = \alpha_{\lambda,\theta} \times I_{x,y} + (\beta_{\lambda,\theta} + NVF_{x,y}) \times w_{x,y} \tag{5}$$

where (x,y) indicates the spatial location. I and w are the decomposed wavelet coefficients of the original image and the logo watermark image. $\alpha_{\lambda,\theta}$ and $\beta_{\lambda,\theta}$ are scaling and embedding factors which are defined as below. $NVF_{x,y}$ is defined in formula (3).

$$\alpha_{\lambda,\theta} = 1 - 0.7\beta_{\lambda,\theta} \tag{6}$$

$$\beta_{\lambda,\theta} = (1 - NVF_{x,y}) \times (I\text{-CSF}) \tag{7}$$

where I-CSF masking is calculated by Eq. (4) and shown in Fig. 3.

Step 4 Inverse transform the DWT coefficients of the original image and convert YCrCb color coefficients into RGB color space to obtain the watermarked image.

4 Experiments

Experiments are designed to evaluate the performance of ICOCOA comprehensively and objectively. We have tested the proposed visible watermarking algorithm on a number of

images by using the widely available color images from USC image database [29] and the experimental images of dimensions 512×512 are shown in Fig. 5 for comparison purpose. The grayscale logo watermarks adopted in the experiments are shown in Fig. 6 where Fig. 6(a) is NCTU logo (school logo) and Fig. 6(b) is IIM logo (department logo).

The detailed analyses are categorized as follows:

4.1 Decision for the watermark weighting value δ

In order to further obtain the perceptual translucence of a clear watermark and find the suitable I-CSF masking values for visible watermarking, δ has been estimated and determined as 0.7 by using game-theory architecture [26, 28] where people can clearly identify the copyright ownership since the embedded patterns are unobtrusive.

The detailed description of the game-theoretic architecture for visible watermarking is as following:

- **Players:**

There are two players in the visible watermarking game: the encoder player and the attacker player.

- **Strategies/Actions:**

The encoder's strategies are six different δ values ($\delta=0.0$, $\delta=0.5$, $\delta=0.7$, $\delta=1.0$, $\delta=1.2$, and $\delta=1.5$). The attacker's actions are 11 different ratio of JPEG2000 compression and the meaning of compression ratio like 0.01 represents 100:1 between the uncompressed image and compressed image. Other settings from 0.10 to 0.02 are with the same operation.

- **The constraints:**

The main requirements of the visible watermarking are the acceptable image quality and the clarity of the embedded patterns for both watermarked image and attacked watermarked image. If the image quality is not satisfactory, the receiver will not accept it and will ask the encoder to

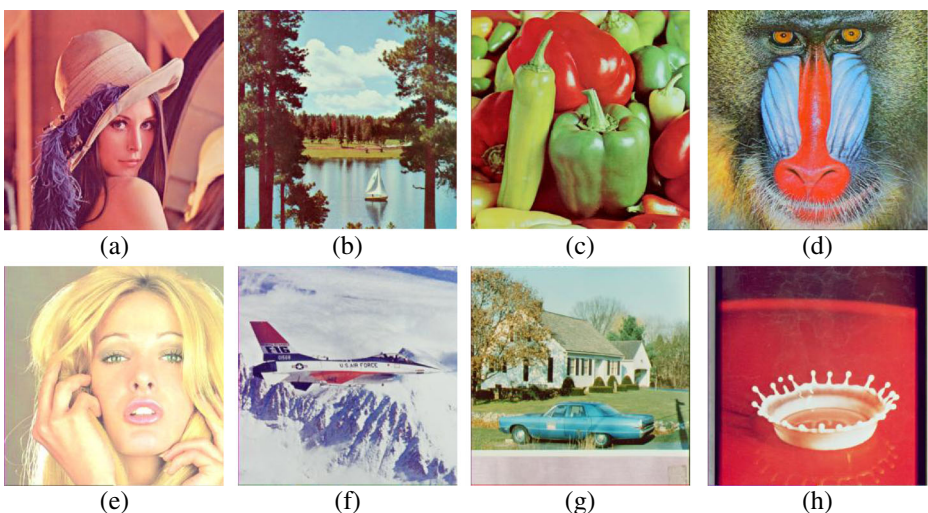


Fig. 5 Test images (a) Lena (b) Lake (c) Peppers (d) Baboon (e) Tiffany (f) F16 (g) House (h) Splash

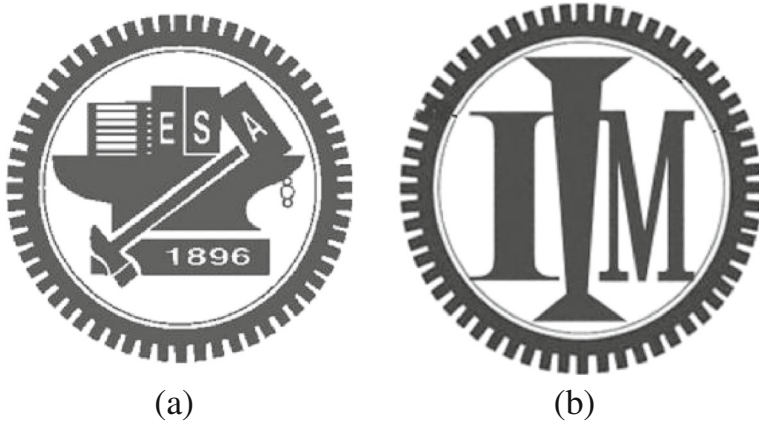


Fig. 6 Two watermark images (a) NCTU logo (b) IIM logo

resend the image. On the other hand, the attacker player cares the erasure or destruction of the watermark with the acceptable image quality. Here a μ value represents the acceptable image quality which is defined in Eq. (8) as the average value of attacker’s payoff function in different strategies and actions.

$$\mu = \begin{cases} \frac{1}{N \times M} \times \sum_{n=1}^N \sum_{m=1}^M f_2(n,m) & , \text{ if } \mu > 0.5 \\ 0.5 & , \text{ otherwise} \end{cases} \tag{8}$$

where N is the encoder’s strategies (six different δ values) and M is the attacker’s actions (11 different ratios of JPEG2000 compression).

- Payoffs:

The payoff function f_1 of encoder player is defined as a function of the strategy profiles e^m (quality assessment metric) and e^5 (correlation) as shown in Eq. (9)

$$f_1(\delta, \text{ratio}) = W_1 \times \frac{1}{4} \times \sum_{m=1}^4 \frac{e_{\delta, \text{ratio}}^m - \min(e_{\cdot, \text{ratio}}^m)}{\text{Max}(e_{\cdot, \text{ratio}}^m) - \min(e_{\cdot, \text{ratio}}^m)} + W_2 \times \frac{e_{\delta, \text{ratio}}^5 - \min(e_{\cdot, \text{ratio}}^5)}{\text{Max}(e_{\cdot, \text{ratio}}^5) - \min(e_{\cdot, \text{ratio}}^5)} \tag{9}$$

where

$$e_{\delta, \text{ratio}}^m = \text{quality assessment metric } (I, I_w)_{\delta, \text{ratio}}^m$$

$$e_{\delta, \text{ratio}}^5 = \text{correlation}((I_w - I), w)_{\delta, \text{ratio}}$$

Note: e^m represents image visual quality metric where e^1 is PSNR (Peak Signal to Noise Ratio), e^2 is VSNR (Visual Signal to Noise Ratio), e^3 is MSSIM (Mean Structural Similarity

Metric) and e^4 is NQM (Noise Quality Measure). The appendix section explains the visual quality metrics PSNR, VSNR, MSSIM and NQM in details. W_1 and W_2 are the weighting parameters for image quality and the robustness of watermark respectively in Eq. (9). Here we assume the watermark robustness plays an important role for the payoff function so we set $W_2=0.6$ and $W_1=0.4$.

- I is the original host image
- w is the logo watermark
- I_w is the watermarked image

The payoff function f_1 is actually a normalized operation from image visual quality metric and correlation in order to get a balanced function value. The encoder’s best response function is $f_1^* = \arg \max_{f_1(\cdot, ratio)}$.

From attacker player point of view, the image visual quality values between the watermarked image and the attacked watermarked image is critical since the attacker expects the lowest image quality after watermark attack. Hence, the payoff function of attacker player, f_2 can be defined as Eq. (10)

$$f_2(\delta, ratio) = \left(\frac{1}{4}\right) \times \sum_{n=1}^4 \frac{e^n_{(\delta, ratio)} - \min(e^n_{(\delta, \cdot)})}{\max(e^n_{(\delta, \cdot)}) - \min(e^n_{(\delta, \cdot)})} \tag{10}$$

where

$$e^n_{(\delta, ratio)} = \text{quality assessment metric}(I_w, I'_w)_{\delta, ratio}^n$$

Note: e^n represents image visual quality metric where e^1 is PSNR, e^2 is VSNR, e^3 is MSSIM and e^4 is NQM.

- I_w is the watermarked image
- I'_w is the attacked watermarked image

The attacker’s best response function is $f_2^* = \arg \min_{f_2(\delta, \cdot)}$.

- Equilibrium Condition

Here we adopt the concept of the Nash equilibrium and analyze the strategies/actions of the players in the system. If there exists a solution profile (f_1^*, f_2^*) where $(f_1^*, f_2^*) = (\arg \max_{f_1(\cdot, ratio)}, \arg \min_{f_2(\delta, \cdot)})$, we can say (f_1^*, f_2^*) is an equilibrium condition result of the game-theoretic architecture for visible watermarking.

Since we need to find the suitable I-CSF masking for the watermark weighting value δ , the Lena image is tested thoroughly under the game-theoretical approach where IIM logo image of Fig. 6(b) is used as the watermark. The visual quality comparison for different δ values of Lena image is illustrated in Fig. 7. We observe that the intensity of watermark pattern is too apparent on the watermarked image of Fig. 7(a.1) ($\delta=0.0$) and Fig. 7(b.1) ($\delta=0.5$) where the PSNR values are below 30 dB. On the other hand, the watermark pattern is too obscure for Fig. 7(e.1) ($\delta=1.2$) and Fig. 7(f.1) ($\delta=1.5$) where the PSNR values are high but the logo watermark cannot be easily identified. To further investigate the effect of δ values, Table 1 tabulates payoff function values for watermarked Lena image under JPEG2000 attack and the best δ is 0.7 under the game-theoretic system. Noticeably, the images of Fig. 7(c.1) and Fig. 7(c.2) does achieve better image quality than others. Similar results are obtained for different host images and the performance is quite alike for $\delta=0.7$. Therefore, $\delta=0.7$ will be applied for the rest of the experiments.



Fig. 7 The visual quality comparison for different δ value of watermarked Lena images. (a.1), (b.1), (c.1), (d.1), (e.1) and (f.1) are watermarked Lena images for $\delta=0, 0.5, 0.7, 1.0, 1.2, 1.5$ respectively. (a.2), (b.2), (c.2), (d.2), (e.2), and (f.2) are close-up images of (a.1), (b.1), (c.1), (d.1), (e.1), and (f.1) respectively. The PSNRs of (a.1), (b.1), (c.1), (d.1), (e.1), and (f.1) are 17.43 dB, 28.86 dB, 32.52 dB, 36.21 dB, 37.67 dB and 39.11 dB respectively

4.2 Visual quality comparison

In order to make a fair comparison with the method from [14, 25], it is better to embed the same watermark for the same cover image. However the watermark used in [14] is not available, we embed the logo watermark from Fig. 6 to make the best effort for performance comparison. The performance analysis can be categorized as follows:

4.2.1 Image quality measure

Image quality measure has become crucial for the most image processing applications. It can evaluate the numerical errors between the original image and the tested image. Several image quality measure metrics have been developed for incorporating the texture sensitivity of the HVS [23]. However, in the real world there is yet no universal standard for an objective assessment of image quality. For generalization purpose, we adopt several common image quality metrics for evaluating ICOCOA method, such as PSNR, VSNR, MSSIM and NQM. The image quality metrics will also be used in the payoff function of game-theoretic architecture and the codes are available at MeTriX MuX Visual Quality Assessment Package [19].

Table 1 Payoff function values for watermarked Lena image under JPEG2000 attack and the ideal selection of (δ , ratio) is (0.7, 0.05) for acceptable image quality threshold

Image: Lena; Watermark: IIM																							
δ	Attacker																						
	0.00	0.10	0.09	0.08	0.07	0.06	0.05	0.04	0.03	0.02	0.01	0.00											
Encoder	0.0	0.40	0.00	0.40	1.00	0.40	0.99	0.40	0.97	0.40	0.96	0.40	0.94	0.40	0.92	0.40	0.89	0.40	0.83	0.40	0.75*	0.40	0.62
	0.5	0.69	0.19	0.72	1.00	0.73	0.97	0.73	0.94	0.73	0.89	0.73	0.85	0.73	0.81	0.72	0.75	0.73	0.63*	0.72	0.46	0.71	0.13
	0.7	0.73*	0.40	0.75*	0.88	0.75*	0.85	0.75*	0.81	0.76*	0.76	0.76*	0.72	0.75*	0.69*	0.74*	0.60	0.74*	0.48	0.73*	0.33	0.71*	0.01
	1.0	0.70	0.70	0.71	0.83	0.71	0.80	0.71	0.75	0.71	0.71	0.71	0.67	0.70	0.64*	0.69	0.55	0.69	0.45	0.67	0.32	0.65	0.00
	1.2	0.66	0.83	0.67	0.82	0.67	0.79	0.67	0.75	0.67	0.70	0.67	0.66*	0.66	0.61	0.66	0.55	0.66	0.45	0.64	0.32	0.63	0.00
	1.5	0.62	0.94	0.63	0.79	0.63	0.76	0.63	0.72	0.63	0.67	0.63	0.63*	0.62	0.59	0.62	0.53	0.63	0.44	0.62	0.32	0.61	0.00

The constraint for attacker of acceptable image quality $\mu=0.63$

The italic values (0.7, 0.05) means the best selection of Nash Equilibrium from encoder's and attacker's payoffs

* means the best selection from encoder's or attacker's payoffs

The tabulated results from Table 2 disclose that ICOCOA watermarking scheme has superior performance than [14] and [25] for most of the image quality measures. This denotes that the fidelity of images from our method is superior to the traditional CSF based methods objectively. Even the PSNR results from ICOCOA are slightly less than Tsai’s method [25], it is widely known that PSNR is the mathematical statistic which only calculates mean square errors between the original and tested images and the PSNR values do not reflect the image fidelity consistently. We have notice this fact and we believe that ICOCOA provides an adaptive embedding algorithm in different subbands to reduce the threshold settings which can achieve better image quality objectively. From Table 2, the results of visual quality metric VSNR, MSSIM and NQM support such observation and the ICOCOA achieves the highest values than others.

4.2.2 Visual quality comparison

We compare the visual quality of the watermarked images for ICOCOA algorithm with Huang and Tang’s [14] and Tsai’s [25] methods. From Figs. 8, 9, and 10, the proposed method has the closest luminance maintenance compared with the original ones which are shown clearly and unobtrusive from the photos. The watermarked images by using [14] and [25] have more bright effect in the unmarked areas. For example, Fig. 8(a), (e), (i) illustrate the original cover images of Lena, Lake and F16 from [29] by embedding NCTU logo of Fig. 6(a), the results of watermarked images from [14] and [25] are compared with the proposed approach and the results are in Fig. 8(b), (c), (d), (f), (g), (h), (j), (k), (l). Similar illustration, Fig. 9(a), (e), (i)

Table 2 Performance summaries of different watermarked color images for both NCTU and IIM logo images

Image	Watermark	PSNR value (dB)			VSNR value (dB)			MSSIM value			NQM value (dB)		
		A	A(2)	A(3)	B(1)	B(2)	B(3)	C(1)	C(2)	C(3)	D(1)	D(2)	D(3)
Lena	NCTU	26.9	31.6	29.2	17.0	21.9	23.9	0.93	0.94	0.94	14.9	21.0	22.5
Lake	NCTU	26.2	30.8	28.3	19.0	24.3	26.7	0.94	0.95	0.95	16.2	22.0	23.6
Peppers	NCTU	26.8	31.4	28.9	17.7	22.5	24.3	0.93	0.94	0.94	16.9	22.7	24.0
Baboon	NCTU	27.1	30.2	26.3	15.9	19.9	21.1	0.95	0.96	0.96	12.6	18.6	20.0
Tiffany	NCTU	28.3	32.0	29.0	12.8	16.7	18.0	0.91	0.93	0.93	8.7	14.3	15.5
F16	NCTU	28.7	31.6	28.6	15.5	19.6	21.4	0.91	0.93	0.93	13.6	19.1	20.5
House	NCTU	28.2	31.0	28.1	15.9	20.0	21.8	0.93	0.95	0.95	13.1	18.9	19.9
Splash	NCTU	25.6	31.3	29.2	18.8	24.6	26.4	0.88	0.91	0.91	13.7	19.3	20.1
Lena	IIM	26.8	32.7	32.5	15.7	21.9	23.0	0.92	0.95	0.95	13.9	20.2	20.9
Lake	IIM	26.0	31.7	31.3	18.0	24.2	26.3	0.93	0.96	0.96	15.2	21.4	22.3
Peppers	IIM	26.8	32.5	32.1	16.6	22.5	23.9	0.92	0.96	0.95	15.8	22.0	22.7
Baboon	IIM	27.2	31.0	28.1	15.2	20.4	21.4	0.94	0.97	0.97	11.5	17.7	18.1
Tiffany	IIM	27.6	32.9	31.8	11.6	17.0	17.7	0.89	0.94	0.94	7.8	13.5	14.0
F16	IIM	28.0	32.4	31.7	14.2	19.5	20.6	0.89	0.94	0.94	12.5	18.1	19.0
House	IIM	27.7	32.0	30.9	15.0	20.3	21.5	0.92	0.95	0.95	12.1	18.2	18.7
Splash	IIM	25.7	32.4	32.6	17.9	24.5	25.5	0.86	0.93	0.93	12.5	18.6	18.6

A, B, C and D are image quality metric of PSNR, VSNR, MSSIM and NQM respectively

(1) is Huang and Tang’s method [14]

(2) is Tsai’s method [25]

(3) is the proposed ICOCOA approach

illustrate the original cover images of Lena, Lake and F16 from [29] by embedding IIM logo of Fig. 6(b), the results of watermarked images from [14] and [25] are compared with the proposed approach and the results are in Fig. 9(b), (c), (d), (f), (g), (h), (j), (k), (l).

To further compare the details on the watermarked images, Fig. 10(a), (e), (i) are the close-ups of original images. Figure 10(b), (f), (j) are the close-ups of Fig. 8(b), (f), (j) by using [14]’s method. Figure 10(c), (g), (k) are the close-ups of Fig. 8(c), (g), (k) by using [25]’s method. Figure 10(d), (h), (l) are the close-ups of Fig. 8(d), (h), (l) by using our proposed method. It is very clear that the watermark’s edges and thin lines are blurred and obtrusive in those images by using the method of [14] and [25] but the watermark patterns in our method still has sharp edge and the logo watermark is evidently embedded. The experimental results indicate that our visible ICOCOA watermarking scheme not only corresponds with a better image quality than the approach of [14, 25] but also provides clear identification of the owner pattern.

4.2.3 JPEG2000 Compression attack

The robustness of the proposed visible watermark technique should be tested for compression attack. JPEG2000 compression is one of the common compression attacks on digital images. For JPEG2000 compression, software from [15] is adopted as the compression tool. Figure 11(f), (l), (r) are the close-up of watermarked images after JPEG2000 compression by ICOCOA method. It is apparent that the logo pattern is still evidently existed and

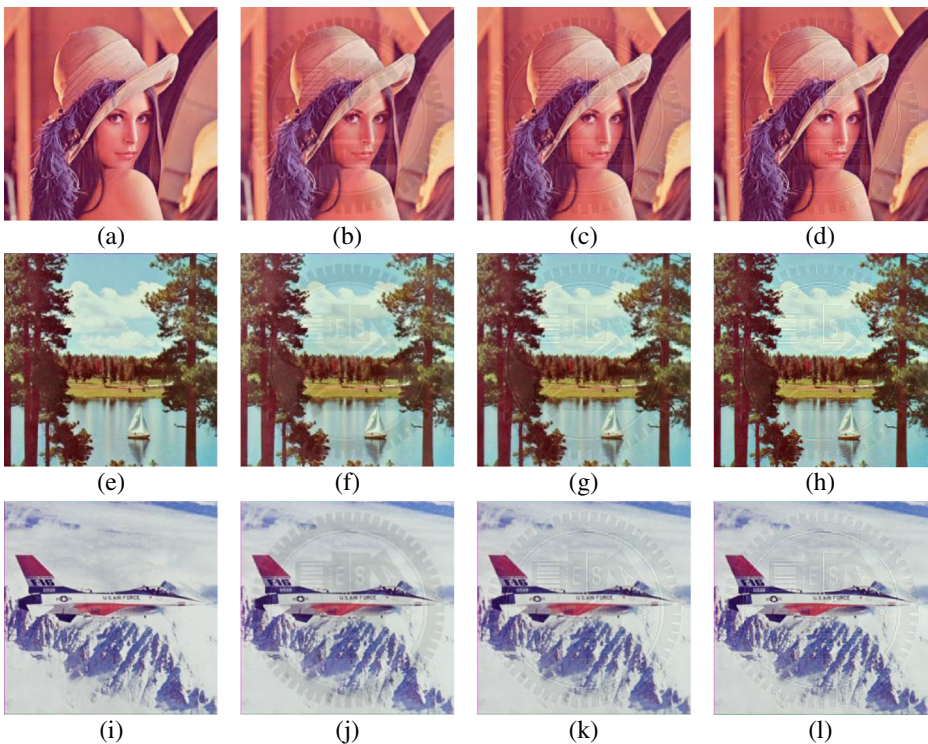


Fig. 8 The visual quality comparison of original and watermarked images by embedding NCTU logo of Fig. 6(a). a, e, i are original Lena, Lake and F16 images respectively. b, f, and j are watermarked images by the method of [14]. c, g, and k are watermarked images by the method of [25]. d, h, l are watermarked images by the ICOCOA method

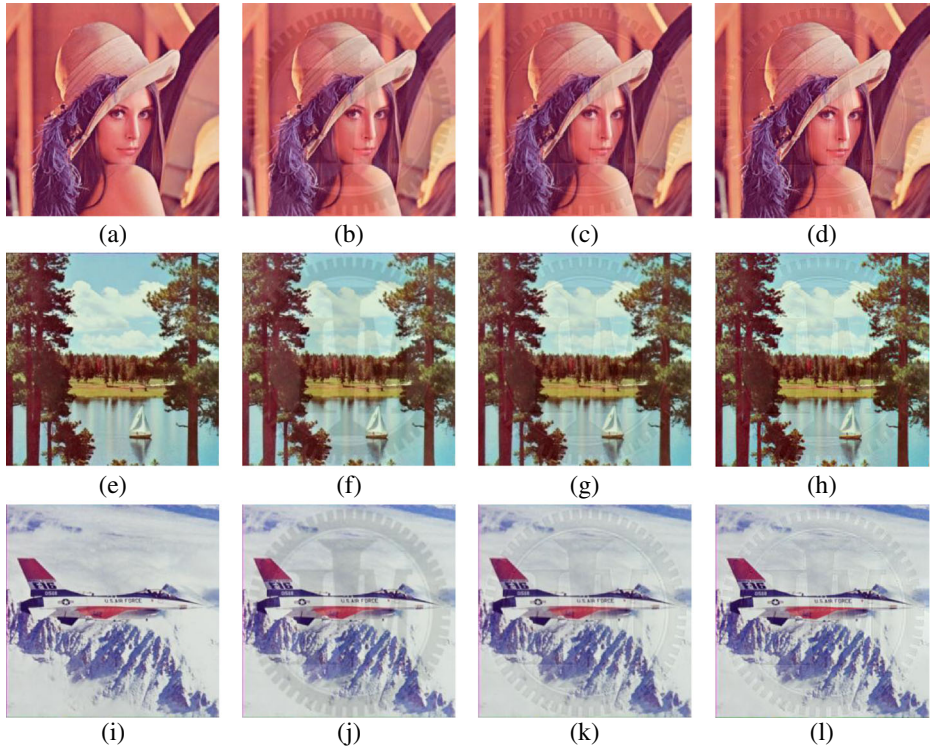


Fig. 9 The visual quality comparison of original and watermarked images by embedding IIM logo of Fig. 6(b). **a**, **e** and **i** are original Lena, Lake and F16 images respectively. **b**, **f**, and **j** are watermarked images by the method of [14]. **c**, **g**, and **k** are watermarked images by the method of [25]. **d**, **h**, **l** are watermarked images by the ICOCOA method

recognized. The values of image quality measures before and after the JPEG2000 compression are tabulated in Table 3. The compression ratio is 100:3 between the uncompressed image and compressed image. There are three rows for the test images. The “before” row means that the image quality measure values are compared between the original image and the watermarked image. The “after” row means the values of image quality measure are compared between the original image and the attacked watermarked image. The “after(wm)” row means the image quality measure values are compared between the watermarked image and the compressed watermarked image (attacked image). From Table 3, the visual image quality measures of VSNR, MSSIM and NQM after attacked are better than those of method [14] and [25]. In the mean time, the PSNR results are still listed for comparison purpose.

To further investigate the attack effect of compression, the visual difference can be illustrated by the close-up comparison in Fig. 11. We observe that the watermark patterns after compression for Fig. 11(f), (l) and (r) are still with sharp edges and the logo watermark can be clearly and easily identified.

4.2.4 Median filtering attack

To further verify the robustness of digital watermarking, the Median filtering attacks of StirMark [24] was performed. Here we illustrate the 7×7 median filtering attack for the

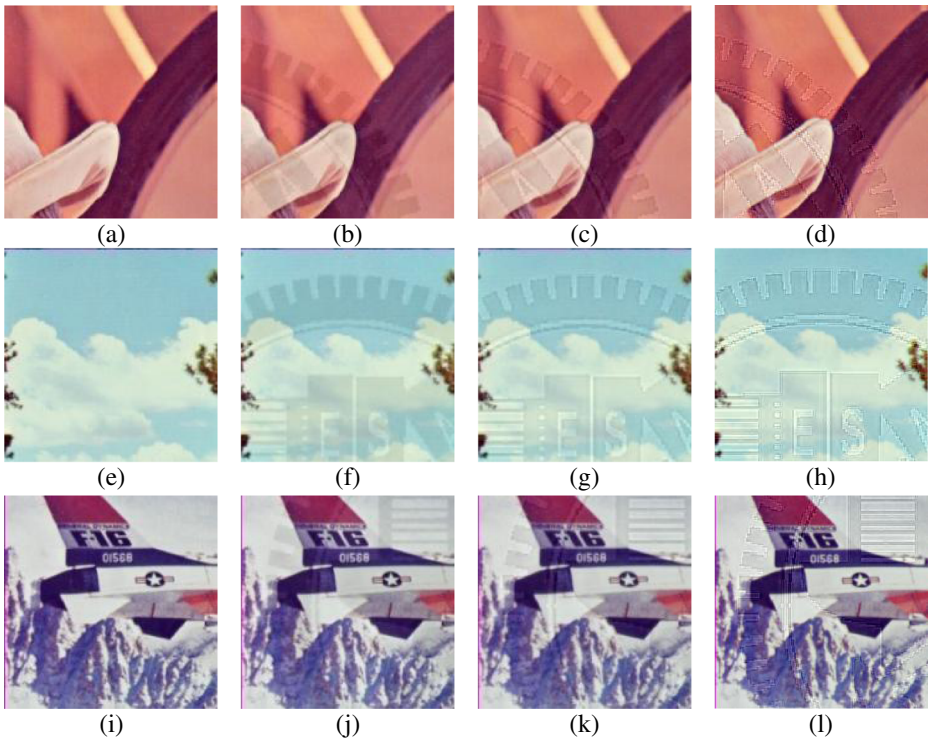


Fig. 10 The visual quality comparison of close-ups for Lena, Lake and F16 images. **a, e and i** are original images. **b, f, j** are watermarked images by the method of [14]. **c, g, k** are watermarked images by the method of [25]. **d, h, l** are watermarked images by the ICOCOA method

demonstration purpose. The performance summaries before and after the median filtering are tabulated in Table 4. The “before” row, the “after” row and the “after(wm)” row of Table 4 are with the same definition in Table 3.

From Table 4, the visual image quality measures of VSNR, MSSIM and NQM after attacked are better than those of method [14] and [25]. To further investigate the attack effect of filtering, the visual difference can be illustrated by the close-up comparison in Fig. 12. While we observe that the watermark patterns after 7×7 median filtering for Fig 12.(a), (b), (c) and (g), (h), (i) carefully, we can notice that only Fig. 12.(f) and (l) are still with visible edges and the logo watermark can be clearly and easily identified. For example, the white edge between English letter “E” and “S” in the logo is preserved for Fig. 12.(f) and (l) but not for Fig. 12.(d), (e) and (j), (k).

4.2.5 Image recovery and watermark removal attack (ICA)

To further examine ICOCOA’s robustness, we have implemented the method of watermark removal attack [21] for verification purpose. Figure 13 illustrates the results of the image recovery attack by the proposed algorithm. In Fig. 13, the logo pattern still exists after the removal attack. The performance summaries before and after the watermark removal attack are tabulated in Table 5. The “before” row, the “after” row and the “after(wm)” row of Table 5 are with the same definition in Table 3.

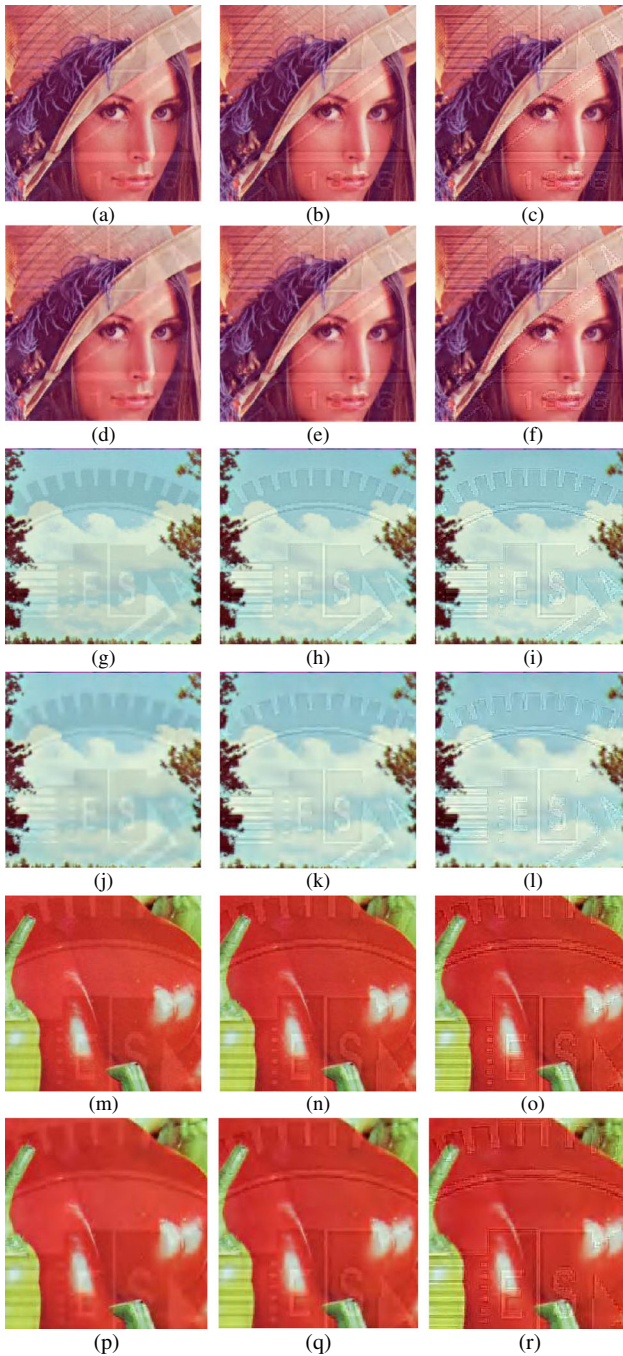


Fig. 11 The visual quality comparison of close-ups for Lena, Lake and Peppers images. **a**, **g** and **m** are watermarked images by the method of [14]. **b**, **h** and **n** are watermarked images by the method of [25]. **c**, **i** and **o** are watermarked images by the ICOCOA method. **d**, **j** and **p** are watermarked images by the method of [14] after JPEG2000 compression. **e**, **k** and **q** are watermarked images by the method of [25] after JPEG2000 compression. **f**, **l** and **r** are watermarked images by the ICOCOA method after JPEG2000 compression

Table 3 Performance summaries of different watermarked color images before and after JPEG2000 for both NCTU and IIM logo images

Image	Watermark	PSNR value (dB)			VSNR value (dB)			MSSIM value			NQM value (dB)			
		A (1)	A (2)	A (3)	B (1)	B (2)	B (3)	C (1)	C (2)	C (3)	D (1)	D (2)	D (3)	
NCTU logo	Lena	Before	26.9	31.6	29.2	17.0	21.9	23.9	0.93	0.94	0.94	14.9	21.0	22.5
		After	24.5	26.8	26.3	17.6	21.3	21.9	0.91	0.93	0.93	14.8	20.6	21.5
		After(wm)	28.3	28.2	27.2	26.4	26.5	24.2	0.97	0.97	0.95	26.9	27.7	26.1
	Lake	Before	26.2	30.8	28.3	19.0	24.3	26.7	0.94	0.95	0.95	16.2	22.0	23.6
		After	23.1	25.0	24.9	19.5	22.2	22.4	0.91	0.92	0.92	16.0	21.1	21.9
		After(wm)	26.2	26.4	25.8	24.6	25.1	24.4	0.95	0.95	0.94	24.4	25.7	24.9
	Peppers	Before	26.8	31.4	28.9	17.7	22.5	24.3	0.93	0.94	0.94	16.9	22.7	24.0
		After	24.5	26.7	26.1	18.7	22.0	22.7	0.91	0.93	0.93	16.9	22.1	23.0
		After(wm)	28.3	28.1	27.2	27.5	27.3	24.8	0.97	0.97	0.96	28.6	28.7	27.7
	Baboon	Before	27.1	30.2	26.3	15.9	19.9	21.1	0.95	0.96	0.96	12.6	18.6	20.0
		After	20.8	21.6	21.5	13.0	14.4	14.9	0.85	0.87	0.88	11.7	16.0	16.6
		After(wm)	22.6	23.2	23.7	15.0	15.8	16.5	0.89	0.90	0.91	17.0	18.2	19.0
	Tiffany	Before	28.3	32.0	29.0	12.8	16.7	18.0	0.91	0.93	0.93	8.7	14.3	15.5
		After	25.5	27.2	26.1	13.4	16.1	16.5	0.89	0.91	0.91	8.6	13.7	14.4
		After(wm)	28.5	28.4	27.6	20.9	20.9	19.5	0.97	0.96	0.95	19.3	19.7	18.5
	F16	Before	28.7	31.6	28.6	15.5	19.6	21.4	0.91	0.93	0.93	13.6	19.1	20.5
		After	25.3	26.6	25.8	15.9	18.3	18.7	0.89	0.92	0.92	13.4	18.4	19.1
		After(wm)	27.9	27.8	26.7	22.8	22.6	21.2	0.96	0.96	0.95	23.0	23.5	22.8
House	Before	28.2	31.0	28.1	15.9	20.0	21.8	0.93	0.95	0.95	13.1	18.9	19.9	
	After	24.2	25.4	24.9	16.0	18.1	17.8	0.90	0.93	0.92	12.8	18.1	18.0	
	After(wm)	26.6	26.8	26.0	20.9	21.6	20.3	0.95	0.95	0.94	21.1	22.6	21.4	
Splash	Before	25.6	31.3	29.2	18.8	24.6	26.4	0.88	0.91	0.91	13.7	19.3	20.1	
	After	24.0	27.2	26.5	19.2	23.9	25.4	0.86	0.89	0.88	13.6	18.8	19.0	
	After(wm)	29.2	28.9	28.0	31.5	31.7	28.2	0.97	0.97	0.95	27.4	26.8	24.5	
IIM logo	Lena	Before	26.8	32.7	32.5	15.7	21.9	23.0	0.92	0.95	0.95	13.9	20.2	20.9
		After	24.4	27.1	27.1	17.0	22.1	22.5	0.90	0.94	0.94	13.8	20.0	20.5
		After(wm)	28.4	28.5	28.6	26.8	27.3	28.0	0.97	0.97	0.97	26.7	27.7	27.7
	Lake	Before	26.0	31.7	31.3	18.0	24.2	26.3	0.93	0.96	0.96	15.2	21.4	22.3
		After	23.0	25.1	25.3	19.0	22.5	23.0	0.89	0.93	0.93	15.0	20.6	21.1
		After(wm)	26.3	26.6	27.1	24.7	25.4	25.8	0.95	0.95	0.95	24.1	25.1	25.5
	Peppers	Before	26.8	32.5	32.1	16.6	22.5	23.9	0.92	0.96	0.95	15.8	22.0	22.7
		After	24.4	27.0	27.0	18.0	22.9	23.2	0.90	0.94	0.94	15.8	21.8	22.2
		After(wm)	28.4	28.5	28.7	28.0	27.9	28.5	0.97	0.97	0.97	28.8	29.3	29.6
	Baboon	Before	27.2	31.0	28.1	15.2	20.4	21.4	0.94	0.97	0.97	11.5	17.7	18.1
		After	20.8	21.7	21.6	12.8	14.6	15.1	0.84	0.88	0.88	10.5	15.8	15.9
		After(wm)	22.6	23.4	24.6	15.2	16.2	16.8	0.90	0.91	0.92	17.0	19.2	19.7
	Tiffany	Before	27.6	32.9	31.8	11.6	17.0	17.7	0.89	0.94	0.94	7.8	13.5	14.0
		After	25.1	27.4	27.1	12.6	17.0	17.0	0.87	0.92	0.92	7.7	13.2	13.5
		After(wm)	28.6	28.7	28.9	21.7	21.9	22.7	0.97	0.97	0.97	19.8	19.6	20.8
	F16	Before	28.0	32.4	31.7	14.2	19.5	20.6	0.89	0.94	0.94	12.5	18.1	19.0

Table 3 (continued)

Image	Watermark	PSNR value (dB)			VSNR value (dB)			MSSIM value			NQM value (dB)		
		A (1)	A (2)	A (3)	B (1)	B (2)	B (3)	C (1)	C (2)	C (3)	D (1)	D (2)	D (3)
House	After	24.9	26.7	26.6	15.2	18.8	19.4	0.87	0.92	0.93	12.2	17.7	18.4
	After(wm)	28.0	28.2	28.3	23.3	23.6	24.1	0.97	0.97	0.96	22.9	24.8	24.2
	Before	27.7	32.0	30.9	15.0	20.3	21.5	0.92	0.95	0.95	12.1	18.2	18.7
	After	24.0	25.5	25.5	15.4	18.4	18.6	0.89	0.93	0.93	11.9	17.4	17.6
Splash	After(wm)	26.6	27.1	27.5	21.0	21.9	22.4	0.96	0.96	0.96	21.5	22.7	23.2
	Before	25.7	32.4	32.6	17.9	24.5	25.5	0.86	0.93	0.93	12.5	18.6	18.6
	After	24.0	27.5	27.8	18.6	24.7	25.3	0.84	0.91	0.91	12.4	18.2	18.2
	After(wm)	29.3	29.3	29.3	32.3	32.9	33.7	0.98	0.98	0.98	27.5	27.9	28.2

A, B, C and D are image quality metric of PSNR, VSNR, MSSIM and NQM respectively

(1) is Huang and Tang’s method [14]

(2) is Tsai’s method [25]

(3) is the proposed ICOCOA approach

Even we have known that PSNR values do not reflect the image fidelity consistently, the values are still listed for comparison purpose in Table 5. From Table 5, we can see that ICOCOA provides an adaptive embedding algorithm in different subbands to reduce the threshold settings and achieves better image quality objectively. The results of visual quality metric VSNR, MSSIM and NQM support such observation and the ICOCOA accomplishes the highest values than others for images under watermark removal attack. Therefore, the robustness of ICOCOA against inpainting attack is superior to other techniques.

Other attacks from [24] are also preformed and the experimental results are consistent with the above findings which indicate our visible watermarking scheme has better visual effect with high visual image quality values than other schemes like [14] and [25]. StrirMark [24] is a widely used attack tool which includes many different attacks such as add_noise, test_convfilter and so on. In summary, an intensive comparison for proposed ICOCOA technique has been illustrated above and we can conclude that the proposed ICOCOA method is more robust with better image quality than the algorithm of [14] and [25].

4.3 Discussion and future researches

There are several issues that the authors would like to address in this session.

- Analysis of different attack actions under game-theory architecture

Currently we only use JPEG2000 compression attack for the estimation of δ value under the game-theory architecture, other attack actions may apply different δ in order to get the best selection of Nash equilibrium condition. Even we have tried several different attacks which results similar selection of δ , this topic could be further investigated as the future research in order to get the more generalized

Table 4 Performance summaries of different watermarked color images before and after 7×7 median filtering for both NCTU and IIM logo images

Image	Watermark	PSNR value (dB)			VSNR value (dB)			MSSIM value			NQM value (dB)			
		A (1)	A (2)	A (3)	B (1)	B (2)	B (3)	C (1)	C (2)	C (3)	D (1)	D (2)	D (3)	
NCTU logo	Lena	Before	26.9	31.6	29.2	17.0	21.9	23.9	0.93	0.94	0.94	14.9	21.0	22.5
		After	20.4	22.2	22.7	14.7	17.4	17.7	0.89	0.91	0.92	14.3	19.4	20.4
		After(wm)	23.2	24.0	22.7	18.7	17.0	18.6	0.95	0.93	0.92	23.5	17.6	23.9
	Lake	Before	26.2	30.8	28.3	19.0	24.3	26.7	0.94	0.95	0.95	16.2	22.0	23.6
		After	19.4	20.9	21.4	14.4	15.9	16.3	0.86	0.89	0.89	15.1	18.9	19.6
		After(wm)	21.9	22.2	21.7	16.3	15.6	17.3	0.92	0.91	0.90	21.3	17.8	22.0
	Peppers	Before	26.8	31.4	28.9	17.7	22.5	24.3	0.93	0.94	0.94	16.9	22.7	24.0
		After	20.1	22.0	22.6	14.5	16.7	17.1	0.91	0.93	0.94	16.1	20.3	20.9
		After(wm)	23.4	24.0	22.6	18.2	16.9	18.2	0.96	0.95	0.94	23.3	19.2	23.9
Baboon	Before	27.1	30.2	26.3	15.9	19.9	21.1	0.95	0.96	0.96	12.6	18.6	20.0	
	After	17.8	18.6	18.9	8.4	9.3	9.5	0.73	0.74	0.75	12.2	15.9	16.5	
	After(wm)	19.4	19.7	20.2	9.4	9.5	10.3	0.78	0.76	0.79	16.9	12.9	19.1	
Tiffany	Before	28.3	32.0	29.0	12.8	16.7	18.0	0.91	0.93	0.93	8.7	14.3	15.5	
	After	22.4	22.5	22.4	11.8	14.4	14.4	0.87	0.90	0.91	7.9	11.2	11.6	
	After(wm)	22.7	21.6	22.5	15.2	13.1	15.2	0.94	0.92	0.91	13.1	10.2	13.4	
F16	Before	28.7	31.6	28.6	15.5	19.6	21.4	0.91	0.93	0.93	13.6	19.1	20.5	
	After	20.9	21.5	21.5	11.7	12.9	13.2	0.86	0.90	0.91	12.4	15.8	16.5	
	After(wm)	21.9	21.7	21.7	14.1	13.1	14.3	0.94	0.92	0.91	17.6	14.9	18.6	
House	Before	28.2	31.0	28.1	15.9	20.0	21.8	0.93	0.95	0.95	13.1	18.9	19.9	
	After	15.6	20.3	20.6	10.5	11.6	11.9	0.85	0.87	0.88	10.9	13.9	14.5	
	After(wm)	21.0	21.1	21.1	12.4	11.9	13.0	0.91	0.89	0.89	14.6	13.1	16.4	
Splash	Before	25.6	31.3	29.2	18.8	24.6	26.4	0.88	0.91	0.91	13.7	19.3	20.1	
	After	19.9	22.3	23.0	16.4	19.8	20.2	0.86	0.91	0.92	13.4	18.2	18.6	
	After(wm)	23.5	24.6	22.9	21.3	19.1	22.0	0.97	0.94	0.93	21.8	16.2	22.0	
IIM logo	Lena	Before	26.8	32.7	32.5	15.7	21.9	23.0	0.92	0.95	0.95	13.9	20.2	20.9
		After	20.5	22.3	22.7	14.2	17.4	17.6	0.88	0.91	0.92	13.7	19.1	19.7
		After(wm)	23.3	23.7	23.4	18.9	16.7	19.7	0.95	0.93	0.95	23.7	16.7	24.6
	Lake	Before	26.0	31.7	31.3	18.0	24.2	26.3	0.93	0.96	0.96	15.2	21.4	22.3
		After	19.6	21.0	21.3	14.2	15.9	16.2	0.85	0.89	0.89	14.4	18.6	19.2
		After(wm)	21.9	22.0	22.3	16.4	15.6	17.5	0.92	0.91	0.93	21.4	17.0	22.4
	Peppers	Before	26.8	32.5	32.1	16.6	22.5	23.9	0.92	0.96	0.95	15.8	22.0	22.7
		After	20.3	20.1	22.6	14.1	16.8	16.9	0.89	0.94	0.94	15.2	20.1	20.4
		After(wm)	23.1	23.8	23.3	18.2	16.7	18.5	0.97	0.95	0.96	23.3	18.2	24.3
Baboon	Before	27.2	31.0	28.1	15.2	20.4	21.4	0.94	0.97	0.97	11.5	17.7	18.1	
	After	17.9	18.6	18.9	8.4	9.3	9.4	0.72	0.75	0.75	11.1	15.3	15.8	
	After(wm)	19.5	19.6	20.7	9.7	9.6	10.4	0.78	0.77	0.81	17.2	12.6	19.5	
Tiffany	Before	27.6	32.9	31.8	11.6	17.0	17.7	0.89	0.94	0.94	7.8	13.5	14.0	
	After	22.5	22.6	22.3	11.2	14.1	14.1	0.85	0.90	0.91	7.1	10.8	11.0	
	After(wm)	22.7	21.4	23.2	15.5	12.9	15.6	0.94	0.91	0.94	13.0	9.6	13.5	
F16	Before	28.0	32.4	31.7	14.2	19.5	20.6	0.89	0.94	0.94	12.5	18.1	19.0	

Table 4 (continued)

Image	Watermark	PSNR value (dB)			VSNR value (dB)			MSSIM value			NQM value (dB)		
		A (1)	A (2)	A (3)	B (1)	B (2)	B (3)	C (1)	C (2)	C (3)	D (1)	D (2)	D (3)
House	After	21.0	21.5	21.5	11.2	12.9	13.0	0.85	0.90	0.91	11.4	15.3	16.0
	After(wm)	22.0	21.5	22.4	14.0	13.0	14.5	0.95	0.92	0.94	17.5	14.1	18.8
	Before	27.7	32.0	30.9	15.0	20.3	21.5	0.92	0.95	0.95	12.1	18.2	18.7
	After	19.7	20.4	20.5	10.3	11.5	11.8	0.83	0.87	0.88	10.2	13.6	14.1
	After(wm)	21.0	20.9	21.7	12.4	11.8	13.0	0.91	0.89	0.91	14.9	12.7	16.6
	Before	25.7	32.4	32.6	17.9	24.5	25.5	0.86	0.93	0.93	12.5	18.6	18.6
Splash	After	20.1	22.4	23.0	16.1	19.8	19.8	0.84	0.92	0.92	12.3	17.8	17.6
	After(wm)	23.5	24.4	23.6	21.4	18.9	22.6	0.97	0.93	0.96	21.8	15.1	22.7

A, B, C and D are image quality metric of PSNR, VSNR, MSSIM and NQM respectively

(1) is Huang and Tang’s method [14]

(2) is Tsai’s method [25]

(3) is the proposed ICOCOA approach

understanding of the best weights in different DWT level and orientation for the watermarked images.

- The wavelet filter selections

2-D DWT for the watermarking is quite effective since the technique carries out as a separable transformation by cascading two 1-D transformations in the vertical and horizontal directions. Since JPEG2000 is also using this approach to compress the images, using non-separable wavelet filters could generate non-directional robustness and this issue can be further investigated for the visible watermarking algorithms.

- The weighting parameters

The weighting parameters W_1 and W_2 in Eq. (9) are 0.4 and 0.6 respectively in this study which are obtained empirically. We can use them flexibly during human objective evaluation under the game-theoretic security system. Therefore, the sensitivity of parameters between the original image, watermarked image and attacked image can be calculated by the analysis of variance (ANOVA) technique in order to get the systematic influence values of the correlation coefficients.

- The quality assessment metrics

Four advanced quality assessment metrics with equal weighting are utilized in this study for the payoff functions of Eqs. (9) and (10) under the game-theoretic architecture. Since there are no universal criteria for the best selection of image quality assessment metrics, this is still an open issue which is worth further study.

- Complexity of ICOCOA with the Human Vision System

The computation complexity of ICOCOA with the Human Vision System is low from the view of mathematical analysis. The whole complexity should be discussed for wavelet transform, I-CSF and NVF calculation, respectively [25].

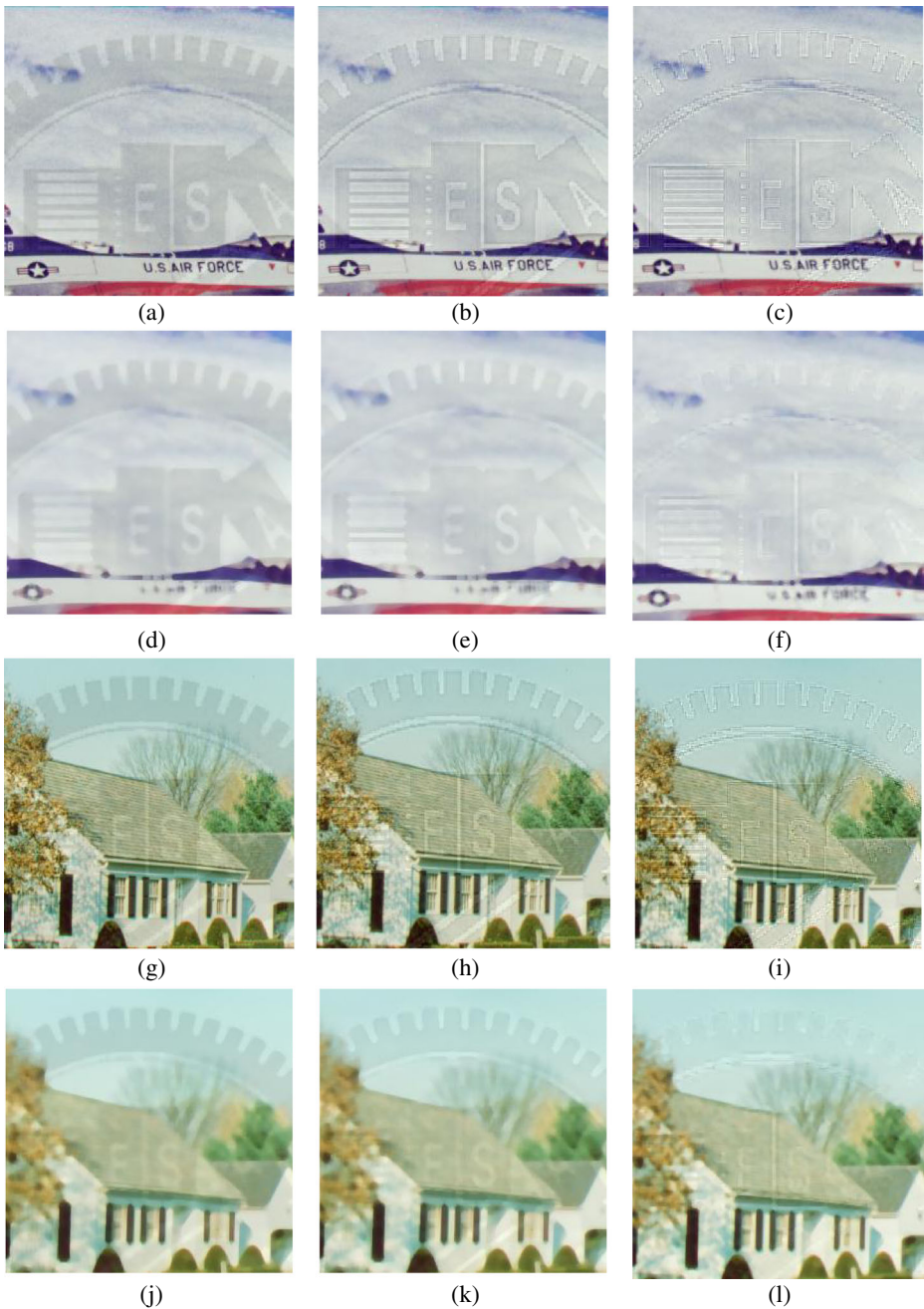


Fig. 12 The visual quality comparison of close-ups for F16 and house images. **a** and **g** are watermarked images by the method of [14]. **b** and **h** are watermarked images by the method of [25]. **c** and **i** are watermarked images by the ICOCOA method. **d** and **j** are watermarked images by the method of [14] after 7×7 median filtering. **e** and **k** are watermarked images by the method of [25] after 7×7 median filtering. **f** and **l** are watermarked images by the ICOCOA method after 7×7 median filtering

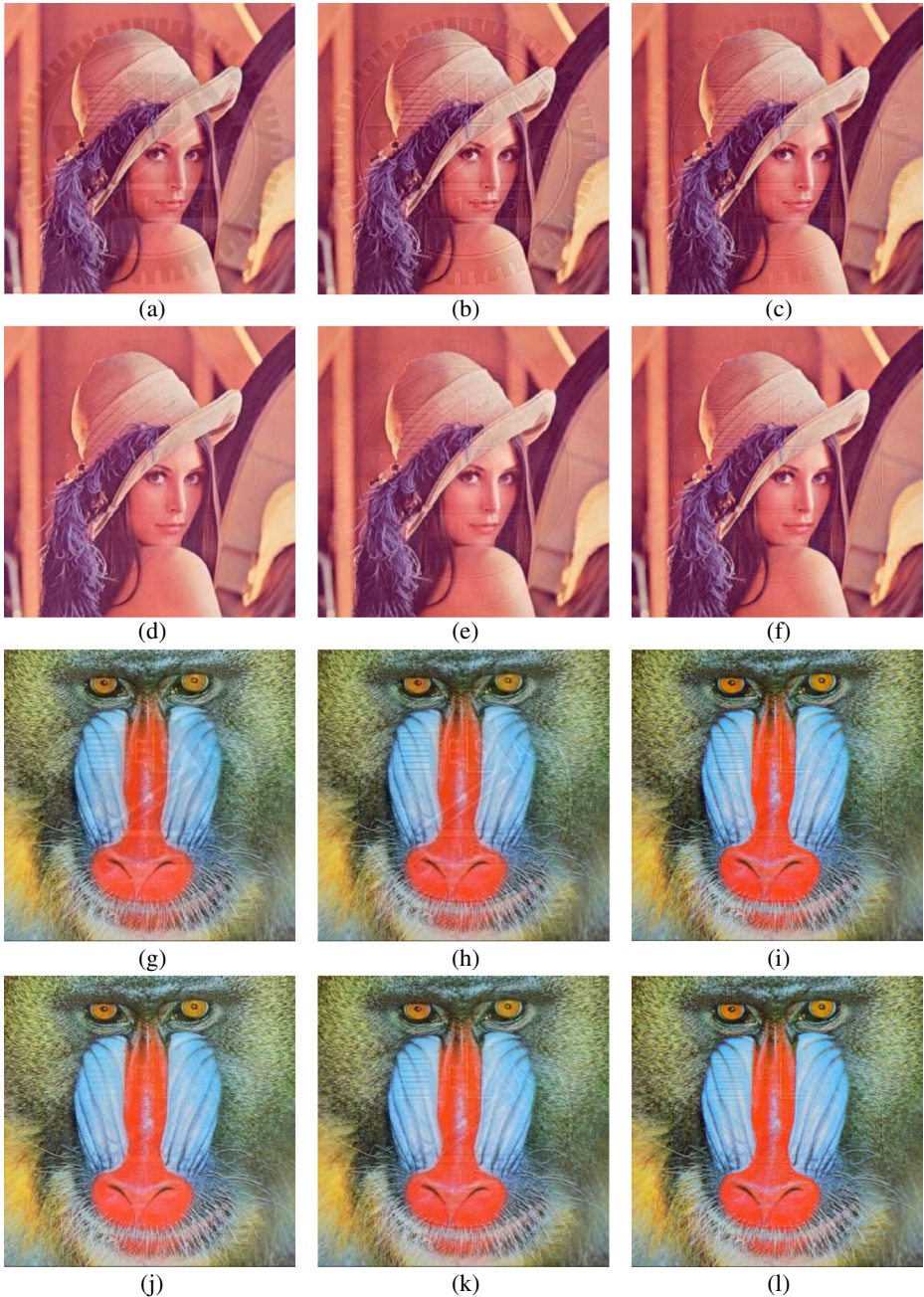


Fig. 13 The visual quality comparison for Lena and Baboon images. **a** and **g** are watermarked images by the method of [14]. **b** and **h** are watermarked images by the method of [25]. **c** and **i** are watermarked images by the ICOCOA method. **d** and **j** are watermarked images by the method of [14] after ICA attack. **e** and **k** are watermarked images by the method of [25] after ICA attack. **f** and **l** are watermarked images by the ICOCOA method after ICA attack

Table 5 Performance summaries for watermarked Lena and Baboon images before and after Watermark removal attack (ICA attack)

Method		PSNR value (dB)			VSNR value (dB)			MSSIM value			NQM value (dB)		
		A(1)	A(2)	A(3)	B(1)	B(2)	B(3)	C(1)	C(2)	C(3)	D(1)	D(2)	D(3)
Lena	Before	26.9	31.6	29.2	17.0	21.9	23.9	0.93	0.94	0.94	14.9	21.0	22.5
	After	21.7	19.8	18.9	24.9	23.7	26.5	0.98	0.96	0.96	18.8	18.9	19.0
	After(wm)	27.8	29.3	32.8	19.4	21.8	25.0	0.94	0.96	0.98	17.6	20.0	22.8
Baboon	Before	27.1	30.2	26.3	15.9	19.9	21.1	0.95	0.96	0.96	12.6	18.6	20.0
	After	20.9	19.0	18.2	22.4	22.0	24.0	0.96	0.96	0.96	15.7	17.9	18.3
	After(wm)	31.3	34.9	42.3	22.1	26.7	33.7	0.98	0.99	0.99	19.4	23.5	27.9

A, B, C and D are image quality metric of PSNR, VSNR, MSSIM and NQM respectively

(1) is Huang and Tang's method [14]

(2) is Tsai's method [25]

(3) is the proposed ICOCOA approach

Suppose the synthesis filters are h (low-pass) and g (high-pass) for wavelet transform. Take $|h|=2N$, $|g|=2M$, and assume $M \geq N$. The cost of the standard algorithm for CDF 9/7 filters [30] is $4(N+M)+2$ and could be sped up by the lifting algorithm in [9] to $2(N+M+2)$. The computation of wavelet transform is linear time mathematics.

On the other hand, I-CSF masking is employed to apply the CSF in the DWT domain, and the associated perceptual weighting function can be pre-calculated for each subband as shown in Fig. 1(b). Therefore, the complexity of I-CSF implementation in ICOCOA becomes the coefficient multiplication from the look-up table. This can be efficiently done in linear-time.

Regarding the complexity of NVF, $\eta(\gamma)$ and gamma function can be pre-calculated by the look-up table when the shape parameters decided. $r(i, j)$ in Eq. (3) is determined by the local means and the local variance which are related to the window size. The complexity of local means and variance is $O(l^2)$, when $l (=2L+1)$ is the window size. In this study, the window size for $L=1$ is 3×3 . Besides, the global variance is obtained for each wavelet subband, and there are 15 subbands after 5 level wavelet decomposition. The total amount of calculation approximately equals to the image size (we can use static array to store the results). Thus, global variance takes $O(n^2)$ computation and the overall time complexity for NVF is no more than $O(n^2)$ ($O(n^2 l^2 + n^2) \approx O(n^2)$), since image width n is much larger than l .

From our simulation [25], the visible watermark embedding process of ICOCOA under Intel Pentium 3.2 GHz, 1 G RAM will need less than 0.5 s to complete for 512×512 testing images. In conclusion, results from the mathematical analysis and simulation show that the ICOCOA complexity is low and suitable for practical applications.

- Different decomposition level of DWT

It is important to decide different weighting values for ICOCOA watermarking. Due to the fact that 9/7 filters [30] are widely accepted, 5 level of DWT decomposition is selected since the basic function amplitudes for a 5-level 9/7 DWT [34] is optimized with less quantization noise. Therefore, its coefficients are utilized for the simulation in this study. In addition, the decomposition level of [14] and [25] is also set at 5, this study adopts 5 level DWT decomposition in order to make a fair comparison. In terms of different decomposition level, it is possible to apply the cross-validation procedure [20] to select the best

decomposition level and the best wavelet filter function based on the input signals, i.e., the cover images. However, huge amount of computation will be required for individual image if such a procedure is applied for each image. Hence, it will be time consuming and result huge significant delay during the communication. Consequently, different parameters of watermarking for each individual image will also create the side information individually. Extra data storage space is needed to preserve those required information. Under such circumstances, certain parameters could be pre-calculated for speedy computation in practice which also makes the copyright protection efficiently.

5 Conclusion

In this study, a novel visible watermarking technique named ICOCOA which is based on exploiting the contrast sensitivity function (CSF) and noise reduction of human vision system has been proposed for the copyright protection. The innovated CSF masking (I-CSF) is designed and fine tuned for watermark embedding which results significant improvement in terms of the image quality, translucence and robustness of the watermarking. In order to determine the best I-CSF masking for the watermarked image, we utilize the game-theoretic architecture for the estimation of the watermark weighting value δ . On the other hand, the contribution of I-CSF is providing better weight perception of wavelet coefficients with low visual distortion for the visible watermark than square function of CSF masking. In addition, the ICOCOA technique can take away the threshold settings in the low wavelet frequency bands for better watermarked images and the translucent watermark pattern is clearly visible and unobtrusive than traditional watermark algorithms. The experimental results demonstrate that the proposed ICOCOA visible watermarking scheme has achieved much better image quality than other schemes in terms of the visual perception and robustness under attacks.

Acknowledgments This work was supported by the National Science Council in Taiwan, Republic of China, under Grant NSC99-2410-H-009-053-MY2 and NSC101-2410-H-009-006-MY2.

Appendix

Formulas of image quality measures

Here are the brief descriptions of the image quality measures (IQM) formulas used for payoff function in this study. Interested readers should refer the references for the detailed information.

A.1. PSNR

PSNR is the most commonly used quality measure for reconstruction of lossy compression codecs such as image compression, image distortion, and so on. The definition of PSNR is as following:

$$PSNR = 10\log_{10}(255^2/MSE) \quad (A1)$$

where MSE is the mean square error between original and tested images.

In general, typical values for the PSNR in lossy image are between 30 dB and 50 dB [35] and a higher PSNR means that the tested image is less degraded and provides a higher image quality.

A.2. VSNR

VSNR, which quantifies the visual fidelity of distorted image. Given the original and distorted images I and K , the proposed metric, which operates for both near-threshold and supra-threshold distortions, estimates visual fidelity via two stages. In the first stage, contrast detection thresholds are computed as described in [4]. If the distortions are below the threshold of detection, the distorted image is deemed to be of perfect visual fidelity ($VSNR=\infty$), and then the algorithm terminates. If the distortions are supra-threshold, a second stage is applied which estimates visual fidelity based on a measure of perceived contrast and a measure of the extent to which the distortions disrupt global precedence.

A.3. MSSIM [32]

The definition of MSSIM is as following:

$$MSSIM(X, Y) = \frac{1}{M} \sum_{j=1}^M SSIM(x_j, y_j) \quad (A3)$$

where X and Y are the reference and the distorted images respectively; x_j, y_j are the image contents at the j th local window and M is the number of local windows in the image.

The SSIM metric is calculated on various windows of an image. The measure between two windows of the size $N \times N$, x and y are two nonnegative image signals. The definition of SSIM is as following:

$$SSIM(x, y) = \frac{(2\mu_x\mu_y + C_1)(2\sigma_{xy} + C_2)}{(\mu_x^2 + \mu_y^2 + C_1)(\sigma_x^2 + \sigma_y^2 + C_2)} \quad (A4)$$

with

μ_x : the average of x ; μ_y : the average of y ;
 σ_x^2 : the variance of x ; σ_y^2 : the variance of y ;
 σ_{xy} : the covariance of x and y ;

C_1 and C_2 are two variables to stabilize the division with weak denominator. Typically, it is calculated on window-sizes of 8×8 .

A.4. NQM [8, 31]

The NQM is based on the Peli's contrast and has shown better performance than the signal-to-noise ratio (SNR), peak SNR (PSNR) and weighted SNR (WSNR).

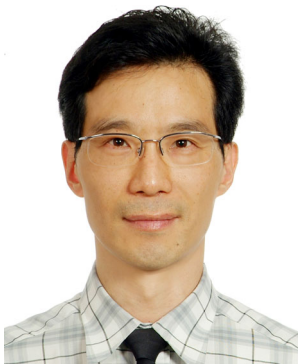
In this quality measurement metric, a degraded image is modelled as an original image that has been modelled as an original image that has been subjective to linear frequency distortion and additive noise injection. These two sources of degradation are considered

independent and are decoupled into two quality measures: a distortion measure (DM) of the effect of frequency distortion, and a noise quality measure (NQM) of the effect of additive noise. The NQM takes into account : (1) variation in contrast sensitivity with distance, image dimensions; (2) variation in the local luminance mean; (3) contrast interaction between spatial frequencies; (4) contrast masking effects. The DM is computed in three steps. First, the frequency distortion in the degraded image is found. Second, the deviation of this frequency distortion from an all-pass response unity gain is computed. Finally, the deviation is weighted by a model of the frequency response of the human visual system.

References

- Alexander SV, Herrigel ZA and Baumgaertner N (1999) "A stochastic approach to content adaptive digital image watermarking." In: Proc. 3rd Int. Workshop Information Hiding, Dresden, Germany, pp. 211–236, Sep. 1999
- An L, Gao X, Xuelong L, Tao D, Deng C, Li J (2012) Robust reversible watermarking via clustering and enhanced pixel-wise masking. *IEEE Trans Image Process* 21(8):3598–3611
- Beegan AP, Iyer LR, and Bell AE (2002) "Design and evaluation of perceptual masks for wavelet image compression." *IEEE Digit Signal Process Workshop*, IEEE CS Press, pp. 88–93, Oct. 2002
- Chandler DM, and Hemami SS (2007) "VSNR: a wavelet-based visual signal-to-noise ratio for natural images." *IEEE Trans Image Process* 16(no. 9):pp. Sep. 2007
- Chen PM (2000) A visible watermarking mechanism using a statistic approach. *5th Int Conf Signal Process Proc* 2:910–913
- Chen JJ, Ng TM, Lakshminarayanan A and Garg HK (2009) "Adaptive visible watermarking using Otsu's Thresholding." *Int Conf Comput Intell Softw Eng* pp. 1–4, Dec. 2009
- Cox JJ, Kilian J, Leighton FT, Shamoon T (1997) Secure spread spectrum watermarking for multimedia. *IEEE Trans Image Process* 6(12):1673–1687
- Damera-Venkata N, Kite TD, Geisler WS, Evans BL, Bovik AC (2000) Image quality assessment based on a degradation model. *IEEE Trans Image Process* 9(4):636–650
- Daubechies, Sweldens W (1998) Factoring wavelet transforms into lifting steps. *J Fourier Anal Appl* 4:247–269
- Gao XB, An LL, Yuan Y, Tao DC, Li XL (2011) Lossless data embedding using generalized statistical quantity histogram. *IEEE Trans Circ Syst Video Technol* 21(8):1061–1070
- Gao XB, Deng C, Li XL, Tao DC (2010) Geometric distortion insensitive image watermarking in affine covariant regions. *IEEE Trans Syst Man Cybern C Appl Rev* 40(3):278–286
- Huang PS, Chiang CS, Chang CP, Tu TM (2005) Robust spatial watermarking technique for colour images via direct saturation adjustment. *IEE Proce Vision Image Signal Process* 152(5):561–574
- Huang CH, Chuang SC, Huang YL, Wu JL (2009) Unseen visible watermarking: a novel methodology for auxiliary information delivery via visual contents. *IEEE Trans Inf Forensics Secur* 4(2):193–206
- Huang BB, Tang SX (2006) A contrast-sensitive visible watermarking scheme. *IEEE Multimed* 13(2):60–66
- JPEG2000 compression, [Online]: <http://www.ece.uvic.ca/~mdadams/jasper/>
- Levický D, Fori's P (2004) Human visual system models in digital image watermarking. *Radio Eng* 13(4):38–43
- Lu CS, Huang SK, Sze CJ, Liao HY (2000) Cocktail watermarking for digital image protection. *IEEE Trans Multimed* 2(4):209–224
- Mannos JL, Sakrison DJ (1974) The effects of a visual fidelity criterion on the encoding of image. *IEEE Trans Inf Theory* 20(4):525–536
- MeTriX MuX visual quality assessment package, [Online]: http://foulard.ece.cornell.edu/gaubatz/matrix_mux/
- Pastia L, Walczaka B, Massarta DL, Reschiglian P (1999) Optimization of signal denoising in discrete wavelet transform. *Chemometr Intell Lab Syst* 48(1):21–34
- Pei SC, Zeng YC (2006) A novel image recovery algorithm for visible watermarked image. *IEEE Trans Inf Forensics Secur* 1(4):543–550
- Preda RO, Vizireanu DN (2010) A robust digital watermarking scheme for video copyright protection in the wavelet domain. *Measurement* 43:1720–1726
- Sheikh HR, Bovik AC (2006) Image information and visual quality. *IEEE Trans Image Process* 15(2):430–444
- StirMark, [Online]: http://www.petitcolas.net/fabien/software/StirMarkBenchmark_4_0_129.zip

25. Tsai MJ (2009) A visible watermarking algorithm based on the content and contrast aware (COCOA) technique. *J Vis Commun Image Represent* 20(5):323–338
26. Tsai MJ and Liu J (2010) “A game-theoretic system security design for the visible watermarking.” In: *Proceedings of the ACM Multimedia 2010 Workshop, Firenze, Italy*, pp.19–23, Oct. 2010
27. Tsai HH, Liu CC (2011) Wavelet-based image watermarking with visibility range estimation based on HVS and neural networks. *Pattern Recogn* 44:751–763
28. Tsai MJ, Liu J, Wang CS (2011) A game-theoretic framework for the security system of visible watermarking. *Expert Syst Appl* 38:5748–5754
29. USC SIPI – The USC-SIPI image database. [Online]: <http://sipi.usc.edu/database/database.html>
30. Villasenor JD, Belzer B, Liao J (1995) Wavelet filter evaluation for image compression. *IEEE Trans Image Process* 4(8):1053–1060
31. Wang Y (2006) “Survey of objective video quality measurements.” Technical report, EMC Corporation Hopkinton
32. Wang Z, Bovik AC, Sheikh HR, Simoncelli EP (2004) Image quality assessment: from error measurement to structural similarity. *IEEE Trans Image Process* 13(4):600–612
33. Wang Y, Pearmain A (2004) Blind image data hiding based on self reference. *Pattern Recogn Lett* 25(15):1681–1689
34. Watson AB, Yang GY, Solomon JA, Villasenor J (1997) Visibility of wavelet quantization noise. *IEEE Trans Image Process* 6(8):1164–1175
35. Wikipedia, the free encyclopedia, [Online]: <http://en.wikipedia.org/wiki/PSNR>
36. Yu PT, Tsai HH, Lin JS (2001) Digital watermarking based on neural networks for color images. *Signal Processing* 81:663–671



Min-Jen Tsai received the B.S. degree in electrical engineering from National Taiwan University in 1987, the M.S. degree in industrial engineering and operations research from University of California at Berkeley in 1991, the engineer and Ph.D. degrees in Electrical Engineering from University of California at Los Angeles in 1993 and 1996, respectively. He served as a second lieutenant in Taiwan army from 1987 to 1989. From 1996 to 1997, he was a senior researcher at America Online Inc. In 1997, he joined the institute of information management at the National Chiao Tung University in Taiwan and is currently a full professor. His research interests include multimedia system and applications, digital right management, digital watermarking and authentication, digital forensic, enterprise computing for electronic commerce applications. Dr. Tsai is a member of IEEE, ACM and Eta Kappa Nu.



Jun Liu is currently a Ph.D. student at the institute of information management, National Chiao Tung University.



Jin-Sheng Yin is currently a Ph.D. student at the institute of information management, National Chiao Tung University.



Imam Yuadi is currently a Ph.D. student at the institute of information management, National Chiao Tung University.